

ELECTROPHORETIC SEPARATIONS OF MONOLAYER PROTECTED CLUSTERS

By

Brian Carl Hixson

Thesis

Submitted to the Faculty of the
Graduate School of Vanderbilt University
in partial fulfillment of the requirements
for the degree of

MASTER OF SCIENCE

in

Chemistry

August, 2009

Nashville, Tennessee

Approved:

Professor David E. Cliffel

Professor Charles M. Lukehart

TABLE OF CONTENTS

Chapter	Page
I. INTRODUCTION	1
1.1 Monolayer Protected Clusters.....	1
1.1.1 Properties of Monolayer Protected Clusters	1
1.1.2 Practical Applications	3
1.1.3 Modification of the Protecting Monolayer	4
1.1.4 Electrophoresis of Monolayer Protected Clusters.....	5
1.2 Capillary Electrophoresis.....	6
1.3 Continuous Free Flow Electrophoresis.....	7
1.4 Summary of Thesis	8
II. EFFECT OF MIXED MONOLAYERS ON THE ELECTROPHORETIC PROPERTIES OF MONOLAYER PROTECTED CLUSTERS	9
2.1 Introduction.....	9
2.2 Experimental Methods.....	10
2.2.1 Reagents and Chemicals	10
2.2.2 MPC Synthesis.....	11
2.2.3 Place-Exchange Reactions	12
2.2.4 Sample Preparation for Capillary Electrophoresis.....	12
2.2.5 Capillary Conditioning.....	13
2.2.6 Capillary Electrophoresis Equipment	13
2.2.7 Ultraviolet-Visible Spectroscopy (UV-Vis)	14
2.2.8 Nuclear Magnetic Resonance Spectroscopy (NMR)	14
2.2.9 Transmission Electron Microscopy (TEM).....	14
2.2.10 Thermal Gravimetric Analysis (TGA).....	15
2.3 Results and Discussion	16
2.3.1 Place-Exchange Reactions and Product Characterization	16
2.3.2 Electrophoretic mobility of Place-Exchanged MPCs	19
2.3.3 Hydrodynamic radius and effective surface charge of MPCs	24
2.3.4 Electrophoretic Mobility of MUA exchanged TMPCs.....	26
2.4 Conclusions.....	31
III. OPTICAL CHARACTERIZATION OF CONTINUOUS FREE-FLOW ELECTROPHORETICALLY SIZE SEPARATED TIOPRONIN MONOLAYER PROTECTED CLUSTERS	32
3.1 Introduction.....	32
3.2 Experimental Methods.....	34

3.2.1 Reagents and Chemicals	34
3.2.2 MPC Synthesis.....	34
3.2.3 Transmission Electron Microscopy (TEM)	35
3.2.4 Thermal Gravimetric Analysis (TGA).....	36
3.2.5 Nuclear Magnetic Resonance Spectroscopy (NMR)	36
3.2.6 Ultraviolet-Visible Spectroscopy (UV-Vis)	36
3.2.7 Near-Infrared Fluorescence	37
3.2.8 Capillary Electrophoresis.....	37
3.2.9 Continuous Free-Flow Electrophoresis (CFFE)	38
3.3 Results and Discussion	39
3.3.1 Synthesis and characterization of MPCs.....	39
3.3.2 Continuous Free-Flow Electrophoresis of Tiopronin MPCs	42
3.3.3 UV-visible absorbance of CFFE fractions.....	42
3.3.4 Near Infrared Fluorescence of CFFE fractions.....	46
3.3.5 Using CE to Characterize CFFE Fractions	49
3.4 Conclusions.....	51

Appendix

CONTINUOUS FREE-FLOW ELECTROPHORESIS OPERATION MANUAL	52
A1 Rationale	52
A2 Instrument History	52
A3 Instrument Theory.....	53
A4 Instrumental Components	55
A4.1 Separation Chamber.....	55
A4.2 Pumping System	58
A4.3 Power Supply	59
A4.4 Fraction Collector	59
A4.5 Cooling System.....	60
A4.6 Outer Casing	60
A5 Instrumental Calibrations and Maintenance	61
A5.1 Pump Calibration	61
A5.2 Checking Flow Profile	64
A5.3 Membrane Replacement	67
A6 Experimental Walkthrough.....	68
A6.1 Buffer and Sample Preparation.....	69
A6.2 CFFE Setup.....	69
A6.3 Running the CFFE	71
A6.4 After CFFE Separation.....	72
REFERENCES	73

LIST OF FIGURES

Figure	Page
1.1 Schematic of CFFE instrument.....	8
2.1 Electropherograms of MPCs and place-exchanged MPC samples displaying differences in migration time and electrophoretic mobility. Black- TMPC 1 migration time 11.5 min, $-3.74 \pm 0.02 \times 10^{-4} \text{ cm}^2 \text{ V}^{-1} \text{ s}^{-1}$. Blue- TMPC 1 place-exchanged with glutathione 21% (migration time 10.5 min, $-3.64 \pm 0.02 \times 10^{-4} \text{ cm}^2 \text{ V}^{-1} \text{ s}^{-1}$) and 46% (migration time 10 min, $-3.55 \pm 0.02 \times 10^{-4} \text{ cm}^2 \text{ V}^{-1} \text{ s}^{-1}$). Red- GMPC 1 migration time 8.5 min, $-3.22 \pm 0.02 \times 10^{-4} \text{ cm}^2 \text{ V}^{-1} \text{ s}^{-1}$. Asterix indicate the neutral marker, mesityl oxide.....	21
2.2 Evaluation of μ_{EP} of MPCs as glutathione concentration was increased in the monolayer. Black- The mobility of TMPC 1 place-exchanged with glutathione decreases linearly up to ~60% glutathione. Red- The electrophoretic mobility of the reverse place exchange of GMPC 1 with tiopronin remains constant at high concentrations of glutathione. The y-axis has been inverted for clarity.....	23
2.3 Electropherograms of TMPC 2 place-exchanged with MUA from 0-65%. T1,T2,T3- electropherogram peaks from TMPC 2 that consist of more narrow size populations of MPCs with electrophoretic mobilities of -3.37, -3.96, $-3.85 \pm 0.02 \times 10^{-4} \text{ cm}^2 \text{ V}^{-1} \text{ s}^{-1}$ respectively. Peaks decrease in intensity as more MUA is exchanged onto the MPC. MUA- electropherogram peak of MUA exchanged MPCs with electrophoretic mobility of $-3.21 \pm 0.02 \times 10^{-4} \text{ cm}^2 \text{ V}^{-1} \text{ s}^{-1}$. Peak increases in intensity with increasing exchange of MUA. Absorbance values have been normalized to correct for variations in sample concentration. Asterix indicate the neutral marker, mesityl oxide.....	29
2.4 Normalized absorbance of peak maxima from Figure 2.3 as a function of mole fraction MUA (χ_{MUA}). T1(Green Triangle)- TMPC 2 MPCs of smallest sizes, $m = -0.079 \text{ R}^2 = 0.98$. T2(Blue Diamond)- TMPC 2 MPCs of larger sizes, $m = -0.051 \text{ R}^2 = 0.92$. T3(Red Circle)- TMPC 2 MPCs of largest sizes. MUA(Black Square)- TMPC 2 MPCs exchanged with MUA, $m = 0.054 \text{ R}^2 = 0.99$	30
3.1 Characterization data for TMPC 3. (A) Broad NMR spectrum of MPC bound tiopronin (Black) overlaid with the narrow spectrum of free tiopronin ligand (Red). The absence of narrow peaks in the NMR spectrum of the TMPCs (Black) indicate the sample is clean. (B) TGA of tiopronin MPCs, 1.52% water, 36.93% organic tiopronin ligand. (C) TEM histogram of MPCs, average diameter $2.07 \pm 0.67 \text{ nm}$. (D) UV-vis spectrum of MPCs with no surface plasmon band present.....	41

3.2	UV-visible spectra of CFFE fractions. (A) Fractions from separation of TMPC 3 at 0.1 mg/mL concentrations indicating no SP band. (B) Fractions 1-13 from separation of TMPC 4/TMPC 5 at 0.1 mg/mL concentrations with no SP band. (C) Fractions 14-35 from separation of TMPC 4/TMPC 5 at 0.1 mg/mL concentrations depicting a SP band.....	44
3.3	Plots of absorbance intensity vs. fraction ID at fluorescence excitation wavelengths. (A) TMPC 3 at 400 nm indicating a trend in increasing intensity from fraction 5 to fraction 30. (B) TMPC 3 at 450 nm indicating a trend in increasing intensity from fraction 5 to fraction 30. (C) TMPC 4/TMPC 5 at 400 nm indicating a trend in increasing intensity from fraction 1 to fraction 35.....	45
3.4	(A) NIR fluorescence of TMPC 3 fractions at 400 nm excitation wavelength. (Inset) Plot of peak intensity vs. fraction ID. (B) NIR Fluorescence of TMPC 3 fractions at 450 nm excitation wavelength. (Inset) Plot of peak intensity vs. fraction ID. (C) NIR Fluorescence of TMPC 4/TMPC 5 fractions at 400 nm excitation wavelength. (Inset) Plot of peak intensity vs. fraction ID.	47
3.5	(A) Plot of fluorescence emission/UV-vis absorbance vs. fraction id for TMPC 3 fractions at 400 nm excitation, indicating higher fluorescence in the earlier fractions. (B) Plot of fluorescence emission/UV-vis absorbance vs. fraction id for TMPC 3 at 450 nm excitation, indicating higher fluorescence in the earlier fractions. (C) Plot of fluorescence emission/UV-vis absorbance vs. fraction id for TMPC 4/TMPC 5 fractions at 400 nm excitation, indicating higher fluorescence in the earlier fractions. 48	
3.6	CE analysis of TMPC 3 fractionated by CFFE. (A) fraction 5, (B) fraction 10, (C) fraction 15, (D) fraction 20, (E) fraction 25, (F) fraction 30, (G) fraction 35, and (H) overlay of fractions. Note that from fraction to fraction peak 1 increases while peak 2 decreases relative to each other. (I) Plot of peak1/peak2 vs. fraction id indicating a near linear trend in the change from peak 1 to peak 2. (*) neutral marker.....	50
A1	Schematic diagram of a simple CFFE separation. Buffer and sample are added at the top of the chamber (Clear and Orange triangles). Analyte with high μ_{EP} (Yellow) migrates towards the oppositely charged electrode faster and analyte with low μ_{EP} (Red). Analytes are collected at the bottom of the chamber in a fraction collector.....	54
A2	Schematic of CFFE instrument. Sample and buffer are introduced in the top of the chamber, while a voltage is applied perpendicularly across the chamber between two plate electrodes. Electrodes are isolated from the main chamber by 0.45 μm nylon membranes. Fresh buffer is continuously circulated over the electrodes to prevent depletion zones in the buffer.....	57
A3	Example Buffer pump calibration curve plotting pump setting versus actual flow rates.....	63

- A4 Picture of CFFE experiment checking the flow profile of solution inside the chamber. Here, flow of solution is non-uniform as evidenced by the clear area at the right of the chamber as well as the bending of the colored streams.65
- A5 Picture of CFFE experiment checking the flow profile of solution inside the chamber. Here, flow of solution appears as uniform bands flowing straight down the chamber with no clear areas.....66

LIST OF TABLES

Table	Page
2.1 Nanoparticle composition of synthesized MPCs	16
2.2 Place Exchange Reactions	18
3.1 Nanoparticle composition of synthesized MPCs	39

CHAPTER I

INTRODUCTION

1.1 Monolayer Protected Clusters

Monolayer protected clusters (MPCs) are metallic (primarily Au, Ag, Pt, Pd) nanoparticles encapsulated in a protecting thiol,¹⁻³ amine,^{4, 5} or phosphine^{6, 7} anchored organic monolayer. MPCs are air stable, and soluble in organic or aqueous solvents depending on the nature of the monolayer. Gold MPCs are of particular interest due to the strong affinity between sulfur and gold atoms, ~ 45 kcal/mol,⁸ which is on the order of a covalent bond. Synthetic strategies yield MPCs that are resistant to agglomeration and decomposition,^{3, 9-11} but typically have a polydisperse range of core sizes (1-8 nm). Due to their size, MPCs bridge the gap between bulk and molecular characteristics of gold or rather, varying sizes of MPCs exhibit bulk characteristics (large MPCs) or become more molecular in nature (small MPCs).^{10, 12} Since the properties of MPCs are size dependent, this could be problematic for practical applications that necessitate particular sizes of nanoparticles or nanoparticles with purely molecular or bulk characteristics.

1.1.1 Properties of Monolayer Protected Clusters

MPCs have innate chemical and physical properties such as optical absorption¹²⁻¹⁴ and fluorescence,¹⁵⁻¹⁸ quantized electrical charging,¹⁹⁻²² and catalytic activity²³ that make them ideal for a variety of applications. UV/Vis spectroscopy of MPCs indicate the presence of a broad surface plasmon absorbance band (SP band) near 520 nm (~ 2.5 eV)

for MPCs with large metal cores but not smaller.²⁴ In fact, it has been shown that as the average core size decreases; the intensity of the SP band diminishes and eventually disappears for MPCs with a diameter less than 2 nm.^{10, 12} The loss of this characteristic SP band as core size decreases has been interpreted as the loss of bulk character for the cluster and the onset of quantum size effects, or rather that the properties of the cluster are appearing less like those of bulk gold and more like individual molecules.¹⁰ MPCs also exhibit unique near-infrared fluorescence (NIRF) properties. Bulk metals, such as gold, have exceedingly small quantum yields on the order of 10^{-10} .²⁵ Gold MPCs, however, have been shown to have significantly higher photoluminescent quantum yields ($\sim 10^{-5}$).¹⁵ Additionally, fluorescence intensity or quantum yield of MPCs increases with decreasing core size, because smaller cores act less like the bulk metal and more like individual molecules.^{17, 26} The exact mechanism for MPC luminescence has yet to be determined. One study suggests that luminescence is due to *sp* to *sp*-like transitions in the δsp band of the gold core, independent of protecting ligand,¹⁵ while recent studies have shown that luminescence is dependent on the passivating ligand and is due to surface electronic excitations and core-to-ligand charge transfers.^{17, 18}

Another unique property of MPCs was observed by Brust *et al.* who measured the conductivity of MPC films with respect to changes in temperature. It was determined that the conductivity of MPC films decreased with decreasing temperature, indicating nonmetallic conduction.¹³ Wuelfing *et al.* also showed that the conductivity of MPCs decreases dramatically as the chain length of the protecting monolayer is increased.²² Another distinctive electronic property of MPCs, specifically alkanethiolate MPCs, is their sub-attoFarad capacitance. These MPCs have a very small capacitance when

dissolved in electrolyte solution, which is attributed to a combination of their small core size and the low dielectric constant of the surrounding organic monolayer of protecting groups.^{19, 20} Using differential pulse voltammetry, Hicks *et al.* was able to experimentally determine that the capacitance of alkanethiolate MPCs increases with increasing core size and decreases with increasing chain length.²⁰ Thus, the effects of core size and chain length on MPC optical and electronic properties become important for applications of MPCs. Applications that require specific optical, electrochemical, or electrophoretic properties would ideally necessitate a specific size of monodisperse MPCs.

1.1.2 Practical Applications

Some MPC applications that have been explored include fluorescence quenching,²⁷ biosensing,^{28, 29} and pseudo-stationary phases.³⁰⁻³² Huang *et al.* reported the use of Au MPCs as fluorescence quenchers with tiopronin or N,N,N-trimethyl-(undecylmercapto)ammonium MPCs would quench the fluorescence of $[\text{Ru}(\text{bpy})_3]^{2+}$, a well known fluorophore.²⁷ Additionally, the ability of MPCs to migrate in an electric field and interact with organic analytes has led to their use as pseudo-stationary phases in capillary electrophoresis. Neiman *et al.* demonstrated increased separation resolution of o-,m-, and p- toluidines and other small organic molecules with the presence gold nanoparticles in the buffer.³⁰ The size dependent properties of MPCs have also led to their use of MPCs as candidates for immunosensor platforms and epitope mapping.^{28, 29} MPCs show potential as platforms for mapping peptide epitopes because their size aids in maintaining the original protein's secondary structure. Through simple place exchange

reactions, Gerdon *et al.* successfully functionalized tiopronin MPCs with linear and looped epitopes of the protective antigen of *B. anthracis* allowing the MPC to mimic the antigen's native structure and show binding with *B. anthracis* antibodies.²⁸ It was suggested that the most faithfully reconstructed conformation of the epitope on an MPC will yield the highest level of biological activity, but the conformation of looped epitopes is dependent on the size of the MPC.²⁸

1.1.3 Modification of the Protecting Monolayer

In addition to core size, the properties of MPCs are also defined by the characteristics of the protecting ligand monolayer. Ligand functionality can affect solubility in organic or aqueous media,²⁴ as well as the electronic and chemical properties of the MPCs.^{11, 14, 18, 20, 22} MPCs are a versatile material that can be modified and functionalized to suit many applications and experimental conditions. To this end, chemistry can be done on MPCs in a wide variety of reactions such as S_N2,^{33, 34} coupling,³⁵ polymerization,³⁶ and place-exchange reactions.^{11, 17, 18, 28, 37} Many post-synthesis techniques for modification of MPC monolayers have been reported.^{33, 35-38} Among these, facile place-exchange reactions provide a simple and effective method for altering monolayer composition and properties by the addition of free thiolates into a solution of MPCs. Place-exchange reactions are completed by co-dissolving MPCs and the exchange ligand in solution and stirring. In place exchange reactions, only a portion of the MPC ligands are exchanged, leaving some of the original ligand still attached to the metal core.^{11, 37, 39} The process can be controlled by adjusting the feed ratio, the molar ratio of exchange ligand to the thiolate ligands bound to the cluster. Low feed ratios have been shown to yield low

product ratios, or lower amounts of place-exchanged ligands.^{37, 39} Modification of the MPC ligand shell can change the optical^{14, 17, 18} and electrochemical^{14, 39, 40} properties of the MPCs on top of size variation.

1.1.4 Electrophoresis of Monolayer Protected Clusters

One of the challenges for using MPCs is that many properties that make them ideal for practical applications are also size dependent. This would require a post-synthetic separation to control nanoparticle size, thereby tuning MPC properties for applications. Several common techniques for size separation of polydisperse samples of MPCs have been explored including high performance liquid chromatography (HPLC),^{41, 42} size exclusion chromatography (SEC),⁴³⁻⁴⁶ and solvent fractionation.^{19, 20} However, these methods suffer from either high loss of material or poor resolution. Electrophoresis, however, is the current gold standard for size separation of MPCs and techniques such as gel,⁴⁷⁻⁴⁹ capillary,⁵⁰⁻⁵⁶ and continuous free-flow⁵⁷ electrophoresis are widely used as tools to narrow the size distribution of water soluble MPCs post-synthesis.

Depending on the nature of the ligand, the MPCs can have an overall positive charge as with N,N,N-trimethyl-(undecylmercapto)-ammonium chloride (TMA) protected MPCs or overall negative charge as with tiopronin protected MPCs. Since the number of protecting ligands is dependent on core size, the overall surface charge varies with change in core size. Larger core sizes require more protecting ligands, affecting the overall charge of the MPC. Thus, techniques such as CE and CFFE that separate based on differences in size and charge are of particular interest for the fractionation of polydisperse MPC samples.

1.2 Capillary Electrophoresis

CE uses a small capillary with a negative potential applied at one end and a positive potential at the other. Charged analytes migrate towards the oppositely charged electrode according to their electrophoretic mobilities, μ_{ep} ($\text{cm}^2 \text{V}^{-1} \text{s}^{-1}$) which can be calculated from equation 1.1.

$$\mu_{eff} = \mu_{ep} + \mu_{eo} \quad (1.1)$$

Where μ_{eff} ($\text{cm}^2 \text{V}^{-1} \text{s}^{-1}$) is the apparent mobility of the analytes being separated, and μ_{eo} ($\text{cm}^2 \text{V}^{-1} \text{s}^{-1}$) is the electroosmotic flow (EOF) of the buffer electrolyte. The μ_{eff} for each analyte is defined in equation 1.2.

$$\mu_{eff} = \frac{L_d / t_m}{V / L_t} \quad (1.2)$$

Where L_d is the length to the detector window (cm), L_t is the total capillary length (cm), t_m is the analyte's migration time to the detector (s), and V is the potential (V). If a neutral marker, an analyte of neutral charge which moves with the buffer, is injected, the EOF can also be calculated using Equation 1.2, which gives μ_{eo} . Knowing μ_{eo} and μ_{eff} , the μ_{ep} can be calculated for each analyte. The straightforwardness of the calculation of μ_{ep} along with the ability to do on-capillary UV detection of analytes makes CE an excellent technique for exploring methods to improve electrophoretic separations of MPCs⁵² as well as determining the electrophoretic mobilities of various types of MPCs and place-exchanged MPCs. The electrophoretic mobility can be related to the effective surface charge on the cluster as shown in equation 1.3.

$$\mu_{ep} = \frac{|Z|e}{6\pi\eta r_H} \quad (1.3)$$

Where Z is the ionic charge of the cluster, e is the charge of an electron, η is the viscosity of the solution, and r_H is the hydrodynamic radius of the particle. Previous CE studies on MPCs have shown that the value obtained for Z is significantly lower than expected if every ionized ligand contributed towards surface charge, and this difference was attributed to shielding of surface charge by the buffer electrolyte.¹¹

1.3 Continuous Free Flow Electrophoresis

Continuous free-flow electrophoresis (CFFE) of MPCs seems to be the ideal separation method as it boasts a high throughput of materials as well as a high separation resolution of material. Until recently, CFFE had been used for the separation of biological molecules such as proteins and cells,⁵⁸⁻⁶² as well as chiral species,⁶³⁻⁶⁶ but a recent study by Peterson *et al.* reported the successful fractionation of tiopronin protected gold MPCs using a commercial CFFE (Figure 1.1).⁵⁷ CFFE has several significant differences from CE that make it potentially more robust. In CFFE, a larger separation area with typical dimensions of 14 x 8 x 3 cm is used compared to the narrow capillary used in CE (~50 μm), allowing higher throughput of sample. Also, buffer and analyte are continuously pumped through the electrophoresis chamber during the separation, generating a constant flow of material as opposed to the discrete injections of CE techniques. Finally, the electric potential is applied perpendicularly to the flow of the analyte, producing a two-dimensional separation. As with its capillary-based counterpart, CFFE fractionates analytes based on their electrophoretic mobilities making CFFE a complimentary preparative technique to CE. The ability to fractionate large quantities (mg) of polydisperse MPCs into more monodisperse samples would be of great use for

practical applications that require discrete sizes of MPCs as well as the study of their size dependent properties.

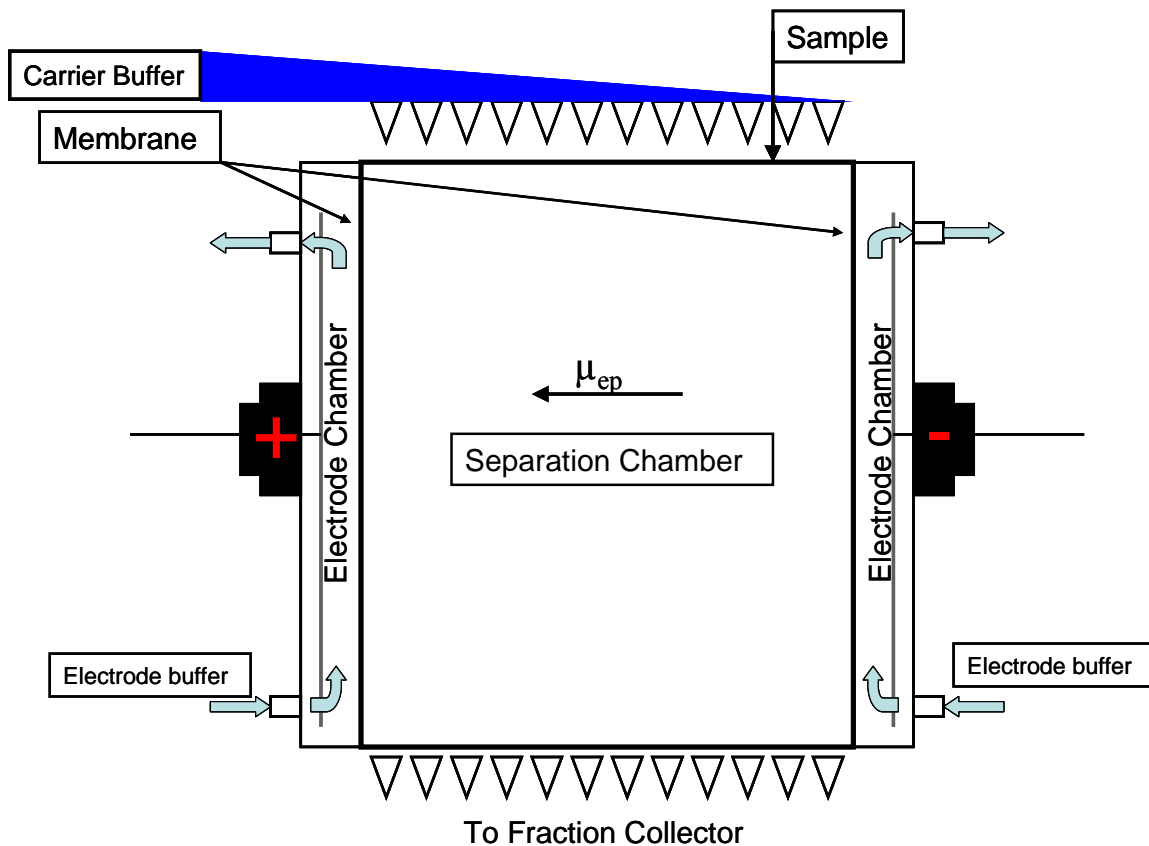


Figure 1.1. Schematic of CFFE instrument. Sample and buffer are introduced in the top of the chamber, while a voltage is applied perpendicularly across the chamber between two plate electrodes. Electrodes are isolated from the main chamber by 0.45 μm nylon membranes. Fresh buffer is continuously circulated over the electrodes to prevent depletion zones in the buffer.

1.4 Summary of Thesis Work

In this thesis, I will first demonstrate the power of CE to study the electrophoretic properties and separations of mixed monolayer protected clusters. Secondly, the use of CFFE to separate larger amounts of MPCs into more monodisperse fractions followed by optical characterization of these fractions will be presented.

CHAPTER II

EFFECT OF MIXED MONOLAYERS ON THE ELECTROPHORETIC PROPERTIES OF MONOLAYER PROTECTED CLUSTERS

2.1 Introduction

The properties of MPCs are partially defined by the characteristics of the protecting ligand monolayer surrounding the gold core. Ligand functionality can affect solubility in organic or aqueous media,²⁴ as well as the electronic and chemical properties of the MPCs.^{11, 14, 18, 20, 22} Many post-synthesis techniques for modification of MPC monolayers have been reported.^{33, 35-38} Among these, facile place-exchange reactions provide a simple and effective method for altering monolayer composition and properties by the addition of free thiolates into a solution of MPCs. Several common techniques for size separation of polydisperse samples of MPCs have been explored including high performance liquid chromatography (HPLC),^{41, 42} size exclusion chromatography (SEC),⁴³⁻⁴⁶ and solvent fractionation.^{19, 20} However, these methods suffer from either high loss of material or poor resolution. Electrophoresis, however, is the current gold standard for size separation of MPCs and techniques such as gel,⁴⁷⁻⁴⁹ capillary,⁵⁰⁻⁵⁶ and continuous free-flow⁵⁷ electrophoresis are widely used as tools to narrow the size distribution of water soluble MPCs post-synthesis. While significant effort has been expended to better understand the electrophoretic properties of gold nanoparticles,^{31, 32, 52,}⁵⁶ there are surprisingly few reports¹¹ of the role of the protecting monolayer on the electrophoretic properties of Au-MPCs. Understanding the effect of ligand exchange on the behavior of MPCs in the presence of an electric field is an important step for a variety of applications, including electrophoretic size separations.

This chapter describes the effects of ligand place-exchange on the electrophoretic properties of water soluble Au-MPCs. Place-exchange reactions of tiopronin-MPCs with common thiolate ligands such as glutathione and 11-mercaptopundecanoic acid (MUA) were performed in aqueous media with varied exchange parameters to generate a wide range of exchanged material. The reaction conditions were altered by changing the molar exchange ratio and reaction time, while conformation and characterization of place-exchange was achieved with ^1H NMR. For comparison the reverse place exchange of synthesized glutathione-MPCs were place-exchanged with tiopronin. The electrophoretic properties of the place-exchange samples were examined *via* capillary electrophoresis, focusing on trends in electrophoretic mobility, effective surface charge and hydrodynamic radius as a function of ligand exchange.

2.2 Experimental Methods

2.2.1 Reagents and Chemicals

$\text{HAuCl}_4 \cdot 3\text{H}_2\text{O}$ was synthesized in house according to literature.⁶⁷ N-(2-mercapto-propionyl) glycine (tiopronin, 99%), glutathione (98% reduced), and mesityl oxide (90%) were purchased from Sigma-Aldrich. Sodium borohydride (98+%), was purchased from Acros, and sodium tetraborate (99.8%), tris (hydroxymethyl) amino methane (Tris), and boric acid were purchased from Fisher. Water was purified in house using a Barnstead NANOpure 18 M Ω Diamond system. All other chemicals were reagent grade and used as received.

2.2.2 MPC Synthesis

Tiopronin protected gold MPCs were synthesized according to established procedures.¹ Briefly, approximately 1 g of $\text{HAuCl}_4 \cdot 3\text{H}_2\text{O}$ was dissolved in 100 mL of a 6:1 methanol:acetic acid solution in a 1 L round bottom flask. Tiopronin was then added (1.44 g, 3 equiv.) to give a ruby colored solution, which quickly faded to pale yellow/clear solution. The temperature was then lowered to 0 °C in an ice bath. In a separate beaker, NaBH_4 (1.11 g, 10 equiv.) was dissolved in a minimum amount of deionized (DI) water and added over approximately 10 seconds to immediately give a black precipitate. The solution was allowed to stir for 30 minutes before removal of the solvent under vacuum. The remaining aqueous solution was acidified to a pH of 1 with concentrated HCl and dialyzed at least 5 days in cellulose ester dialysis tubing (Spectra/Por, 10,000 MWCO) changing the water twice daily. The sample was then extracted from the tubing, and filtered through a fine glass frit. The collected black solution was then dried under vacuum to yield a black flaky solid.

Synthesis of glutathione protected gold MPCs was achieved according to literature.^{47, 48} Briefly, approximately 1 g of $\text{HAuCl}_4 \cdot 3\text{H}_2\text{O}$ was dissolved in 80 mL of methanol and sparged under nitrogen for 1 hour. Glutathione (2.33 g, 3 equiv.) was dissolved in 40 mL of degassed DI water and was added to the methanol solution rapidly forming a milky white solution which was stirred for 15 minutes. The precursor was then reduced with sodium borohydride (1.00 g, 10 equiv.) dissolved in 10 mL of DI water to form a black precipitate. The solution was allowed to stir for 30 minutes before being dried on a rotary evaporator. The resulting black solid was cleaned by dissolving it in a minimum amount of water and drop cast into 500 mL of methanol to rinse out left over

starting materials. This clean up procedure was repeated several times until the sample was confirmed clean using ^1H NMR by noting the absence of sharp peaks characteristic of unbound ligand in favor of broad peaks typical of MPCs.

2.2.3 Place-Exchange Reactions

MPCs (5-20 mg) were dissolved in 10 mL of 20 mM pH 9.3 sodium borate buffer and stirred. An appropriate amount of the exchange ligand was then added to the solution and was allowed to stir anywhere from 1 hour to 5 days depending the degree of desired place-exchange. Un-exchanged ligand was then removed using 10k MWCO centrifuge filters (Amicon Ultra regenerated cellulose) and rinsing several times with DI water. The resulting products were analyzed by ^1H NMR spectroscopy to confirm purity and extent of place-exchange.

2.2.4 Sample Preparation for Capillary Electrophoresis

Approximately 1 mg of MPCs was weighed out and placed in a 2 dram vial and dissolved to a concentration of 1 mg/mL with 20 mM sodium borate buffer (pH = 9.3). 1 μL of a neutral marker solution (990 μL buffer, 10 μL mestiyI oxide) was then added and the solution was sonicated. Samples were filtered though 0.2 μm nylon syringe filters just prior to injection.

2.2.5 Capillary Conditioning

New capillaries were rigorously conditioned prior to initial use by hydrodynamically flushing at 30 psi with DI water (5 min), 1.0 M NaOH (30 min), 0.1 M NaOH (30 min), DI water (50 min), and finally 20 mM (pH 9.3) sodium borate running buffer (30 min). Before each experiment, the capillary was washed with a less rigorous treatment of 0.1 M NaOH, DI water, and running buffer for 5 minutes each at 30 psi.

2.2.6 Capillary Electrophoresis Equipment

Capillary electrophoresis experiments were carried out on a Beckman Coulter P/ACE MDQ capillary electrophoresis instrument with a single wavelength UV detector set at 214 nm. Experiments were conducted in a fused silica capillary (50 μm i.d., 362 μm o.d., and 60 cm total length (50 cm to the detection cell) from Polymicro (Phoenix, AZ). The MPC samples were injected hydrodynamically (5 psi for 5 s) at the anode and were detected near the cathode. All experiments were run in positive mode under a constant voltage of 30 kV with the capillary cooled to 25 $^{\circ}\text{C}$. Each experiment was performed a minimum of three times and the data were analyzed using OriginPro 7.5. Data shown in electropherograms have been baseline corrected to remove drift. Additionally, peak intensities were normalized at 300 nm to correct for minor differences in concentration using a separate UV-vis spectrophotometer to account for variations in sample concentration from sample to sample.

2.2.7 UV-Vis Spectroscopy

UV-Vis spectra were obtained of MPC samples on a Cary 100 Bio UV-vis spectrophotometer in the range of 300-800 nm. Samples were prepared at concentrations around 0.2 mg/mL in DI water or buffer.

2.2.8 NMR

For solid samples, approximately 20 mg of sample was weighed into an NMR tube and dissolved in ~ 600 μ L of D₂O. Samples in aqueous solution were concentrated and 2-3 drops of D₂O was added. Spectra were obtained on a 400 MHz Bruker NMR collecting at least 40 scans with a d1 delay of 1.5 seconds. A double WATERGATE pulse program was used for water suppression.

2.2.9 TEM

Samples were prepared by dissolving a small amount of TMPCs in 1 mM HCl and diluting the sample until the faint brown color was barely visible. One drop was then placed onto 400 mesh ultrathin carbon flim/holey carbon grids (Ted Pella, Redding, CA, Product # 01824) and allowed to air dry overnight. TEM images were obtained on a Phillips CM20 electron microscope operating at 200 kV at magnifications of 200Kx and 400Kx. The negatives were developed and digitized in Adobe Photoshop for measurement. Cluster diameters were measured along the major elliptical axis using ImageJ version 1.41 (available at <http://rsbweb.nih.gov/ij/>).

2.2.10 Thermal gravimetric analysis

The organic composition was determined using TGA (ISI TGA 1000, Instrument Specialists Inc. Twin Lakes, WI). Prior to analysis, samples were dried under vacuum overnight to remove moisture. Typical experiments consisted of 5-10 mg of dry MPCs in a platinum pan under a N₂ flow of ~60 mL/min. Data was recorded between 20 – 900 °C at a rate of 20 °C/min. A brittle, gold solid of remained after analysis.

2.3 Results and Discussion

2.3.1 Place-Exchange Reactions and Product Characterization

Tiopronin and glutathione protected MPCs were synthesized as described in the experimental methods section and characterized *via* NMR, TGA, TEM and UV-vis spectroscopy to determine purity and composition of the MPCs. For the experiments described here, two separate batches of tiopronin MPCs (TMPCs) and one batch of glutathione MPCs (GMPCs) were prepared with diameters of 2.5 ± 0.6 , 2.9 ± 1.1 , and 3.1 ± 1.2 nm, respectively (Table 2.1). It is important to note that the MPCs produced by this synthesis were not a single size, but rather a range of sizes typically around 1-5 nm. As a result, the data in Table 2.1 represents the *average* composition of MPCs in each batch. For best comparison of results, TMPC 1 was used exclusively for place-exchanges with glutathione, while TMPC 2 was used only for exchange with 11-mercaptoundecanoic acid (MUA). In the case of the GMPCs, the average size of the MPCs was larger than those of the TMPCs, but the difference between sizes were still within the relative error of each other and so comparison of place-exchange reactions using these MPCs is possible.

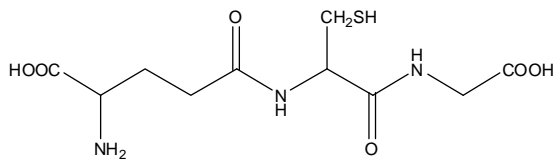
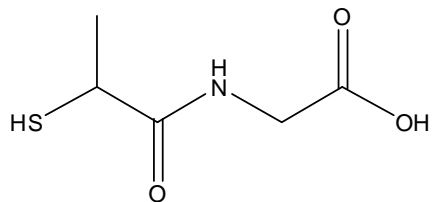
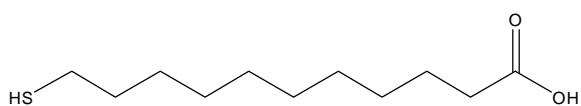
Table 2.1. Nanoparticle composition of synthesized MPCs

Batch ID	Ligand type	Composition d ^a , %O ^b	Average molecular formula
TMPC 1	Tiopronin	2.5±0.6, 26%	Au ₃₀₈ TiO ₁₂₂
TMPC 2	Tiopronin	2.9±1.1, 36%	Au ₅₀₅ TiO ₂₉₃
GMPC 1	Glutathione	3.1±1.2, 38%	Au ₆₁₉ Gluta ₂₄₄

^a Diameter in nm with standard deviation of gold core as measured from TEM. ^b Percent organic from TGA data.

Place-exchange reactions were performed on these batches of MPCs according to the literature^{11, 37} and as described in the experimental methods section. The amount of exchange ligand and the length of time for exchange were controlled in order to generate a wide range of exchange percentages for CE experiments. A summary of place-exchange reactions completed is given in Table 2.2. The extent of exchange was determined using ¹H NMR by comparing the relative integrated values of discrete original-ligand and exchange-ligand peaks and adjusting the average molecular formula of the original MPC material accordingly. From Table 2.2, it can be noted that longer chain ligands exchanged more readily onto short chain capped MPCs than the reverse. In the same range of molar exchange ratios, tiopronin protected MPCs (TMPC 1) were place-exchanged with glutathione between 15% and 95% and glutathione protected MPCs (GMPC 1) were place-exchanged with tiopronin between 2% and 37%, indicating that the exchange of longer ligands with short was less efficient. This was expected as shorter chain lengths of thiolates are thought to have lower thermodynamic stability on the nanoparticle surface.^{37, 68} Additionally, at high ratios of exchange ligand (e.g. 1:10, 1:20) it was far more likely that place-exchange products would precipitate out of solution and irreversibly agglomerate. As a result, whenever possible, the length of exchange time was minimized to reduce the chance of agglomeration. For TMPC 2 exchanged with MUA, exchange ratios above 1:1 were unstable and agglomerated in aqueous solution. MPCs exchanged at 1:1 MUA were exchanged for only one hour and CE experiments were performed the same day of synthesis to minimize loss of product. At lower amounts of exchange, MPCs remained soluble with no visible agglomeration for weeks.

Table 2.2. Place Exchange Reactions

Starting MPC	Exchange Ligand	Exchange Conditions Ratio(OL:EL) ^a , Time ^b	Percent Exchanged ^c
TMPC 1		1:20, 1 week 1:20, 1 week 2:1 , 3 days 3:1 , 3 days 3:1 , 1 days 3:1 , 1 day 3:1 , 1 hour 10:1 , 1 hour 15:1 , 1 hour 20:1 , 1 hour	95% 88% 56% 55% 48% 47% 46% 21% 17% 15%
GMPC 1		1:10, 1 day 1:10, 1 hour 1:5 , 1 hour 1:1 , 1 day 1:1 , 1 hour 10:1 , 1 hour 20:1 , 1 hour	37% 13% 13% 18% 20% 5% 2%
TMPC 2		1:1 , 1 hour 2:1 , 1 hour 3:1 , 1 hour 5:1 , 1 hour 10:1 , 1 hour 20:1 , 1 hour	65% 44% 16% 10% 5% 4%

^a Molar ratio of originally bound ligand (OL) to free ligand in exchange solution (EL). ^b Length of exchange reaction until quenched by centrifugation filtration. ^c Percentage of cluster-bound ligands exchanged as determined by ¹H NMR.

2.3.2 Electrophoretic mobility of Place-Exchanged MPCs

Templeton *et al.*¹¹ first reported the effect of monolayer modification on the electrophoretic properties of MPCs in 1999 where tiopronin-MPCs were modified *via* EDC coupling with N-(Methyl)-N'-(ethylamine)-viologen dinitrate (MEAV⁺²(NO₂⁻)₂). This modification resulted in a significant change in the migration time of the MPCs in capillary electrophoresis, altering the electrophoretic properties of the MPC through monolayer modification. To our knowledge, no further work has been published on this topic, yet electrophoretic techniques continue to be of great interest in the area of MPC size separation. Therefore, it is critical to fully understand the effects of the protecting monolayer on the electrophoretic properties of MPCs.

In capillary electrophoresis experiments, the electrophoretic mobility, μ_{EP} , of nanoparticles can be calculated from equation 2.1.

$$\mu_{EFF} = \mu_{EO} + \mu_{EP} \quad (2.1)$$

Where μ_{EFF} is the effective electrophoretic mobility of the sample and μ_{EO} is the electroosmotic flow of the buffer as indicated by the addition of a neutral marker to the sample.⁶⁹ The μ_{EFF} and μ_{EO} were calculated directly from the capillary electropherograms using equation 2.2.

$$\mu_{(EO,EFF)} = \frac{(L_t)(L_d)}{(V)(t_m)} \quad (2.2)$$

Where L_t and L_d are the capillary's total length and length to the detector, respectively, V is the voltage across the capillary (typically 30 kV), and t_m is the migration time.⁶⁹ Capillary electropherograms of TMPC 1, GMPC 1, and glutathione exchanged TMPC 1 nanoparticles have been overlaid in Figure 2.1 for comparison. There is a noticeable difference in migration time between TMPC 1 at 11.5 minutes (black) and GMPC 1 at

8.5 minutes (red) which directly translates to electrophoretic mobilities of -3.74 ± 0.02 and $-3.22 \pm 0.02 \times 10^{-4} \text{ cm}^2 \text{ V}^{-1} \text{ s}^{-1}$, respectively. Batches of TMPC 1 that have been place-exchanged 21% and 46% with glutathione appear at migration times of 10.5 and 10 minutes (blue) with electrophoretic mobilities of -3.64 ± 0.02 and $-3.55 \pm 0.02 \times 10^{-4} \text{ cm}^2 \text{ V}^{-1} \text{ s}^{-1}$, respectively, giving an overall migration and electrophoretic mobility order of GMPC 1 > 46% > 21% > TMPC 1. Additionally, most TMPC batches synthesized have two or three clear peaks or shoulders indicative of several populations of narrower size distributions than the original sample. For nanoparticles in this size range, it has been shown that MPCs migrate in order from largest to smallest in capillary zone electrophoresis.^{31, 56} This is consistent with previous work by Peterson *et al.*⁵⁷ which determined that the smaller MPCs have a higher electrophoretic mobility than the larger and thus would be last to reach the detector in capillary electrophoresis. GMPCs typically display only one CE peak under the similar conditions as shown in Figure 2.1. If the pH is lowered to between 5 and 6, multiple peaks are observed, however, migration times and peak shapes are irreproducible from run to run. This was attributed to protonation of a carboxylic acid on glutathione as the solution pH fluctuates near its pK_a . Templeton *et al.*¹ demonstrated with a similar thiolate, that the pK_a of ligands bound to a gold cluster was on average 2 units higher than the free ligand. Thus, a carboxylic acid functional group on glutathione with a pK_a of 3.59 would be ~ 5.59 when bound to the gold core. Thus, minor changes in the buffer pH when the pH approximates the pK_a , result in significant changes in number of protonated —COOH groups on each cluster which in turn dramatically effects the migration and separation of the MPCs.

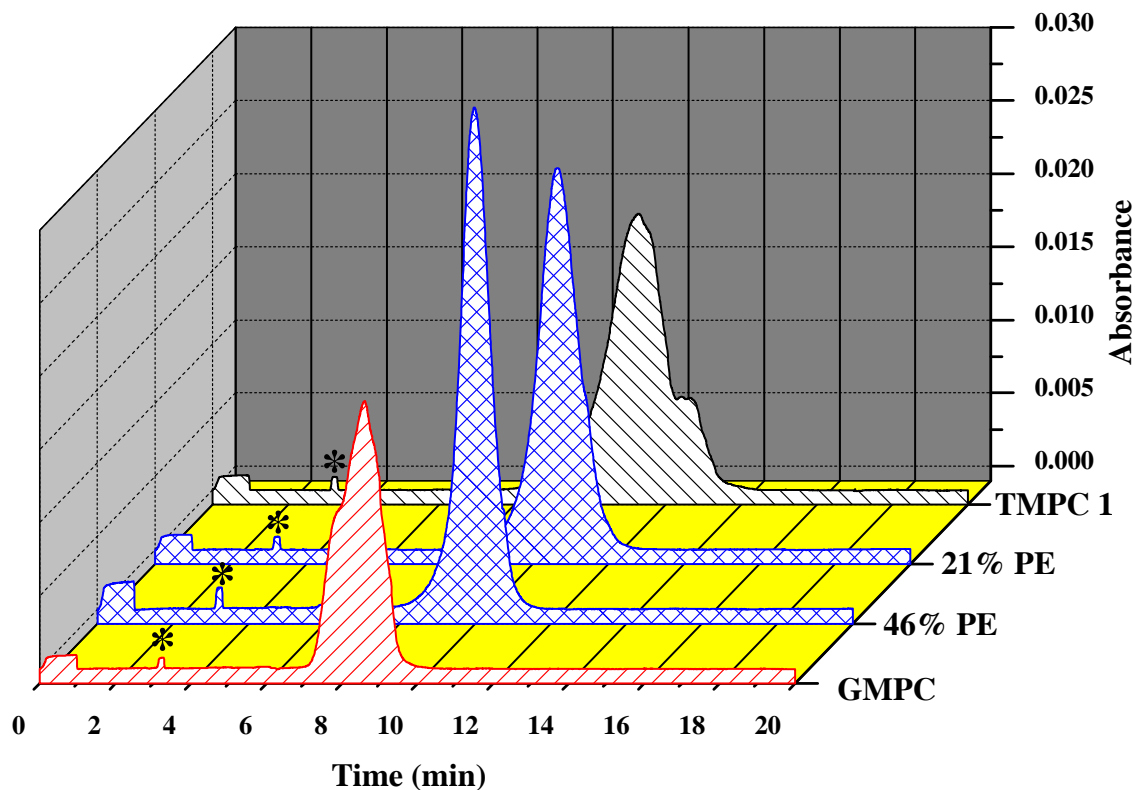


Figure 2.1. Electropherograms of MPCs and place-exchanged MPC samples displaying differences in migration time and electrophoretic mobility. **Black-** TMPC 1 migration time 11.5 min, $-3.74 \pm 0.02 \times 10^{-4} \text{ cm}^2 \text{ V}^{-1} \text{ s}^{-1}$. **Blue-** TMPC 1 place-exchanged with glutathione 21% (migration time 10.5 min, $-3.64 \pm 0.02 \times 10^{-4} \text{ cm}^2 \text{ V}^{-1} \text{ s}^{-1}$) and 46% (migration time 10 min, $-3.55 \pm 0.02 \times 10^{-4} \text{ cm}^2 \text{ V}^{-1} \text{ s}^{-1}$). **Red-** GMPC 1 migration time 8.5 min, $-3.22 \pm 0.02 \times 10^{-4} \text{ cm}^2 \text{ V}^{-1} \text{ s}^{-1}$. Asterix indicate the neutral marker, mesityl oxide.

Figure 2.2 indicates that there is a clear trend in the electrophoretic mobility as the percentage of glutathione exchanged onto the TMPC is increased. The electrophoretic mobility decreased linearly from 0 to ~60% glutathione exchange (black boxes) with a slope of $4.5 (\pm 0.3) \times 10^{-7}$ and $R^2 = 0.995$. At higher percentages of glutathione, the mobility starts to level off. However, place-exchange reactions at high concentrations of exchange ligand frequently agglomerated and were unviable for CE experiments. The mobility trend at high percentages of glutathione was instead examined by performing the reverse place-exchange of tiopronin onto GMPCs. As shown in Figure 2.2, the electrophoretic mobility of GMPC 1 exchanged with tiopronin remained fairly constant across the range of 80-100% glutathione (red circles). The overall electrophoretic mobilities of the GMPC 1 samples were lower than those of the TMPC 1 based place-exchanges with similar amounts of glutathione present. This difference was attributed to the larger average core size of GMPC 1 (3.13 nm) compared to TMPC 1 (2.48 nm) as shown in Table 2.1.

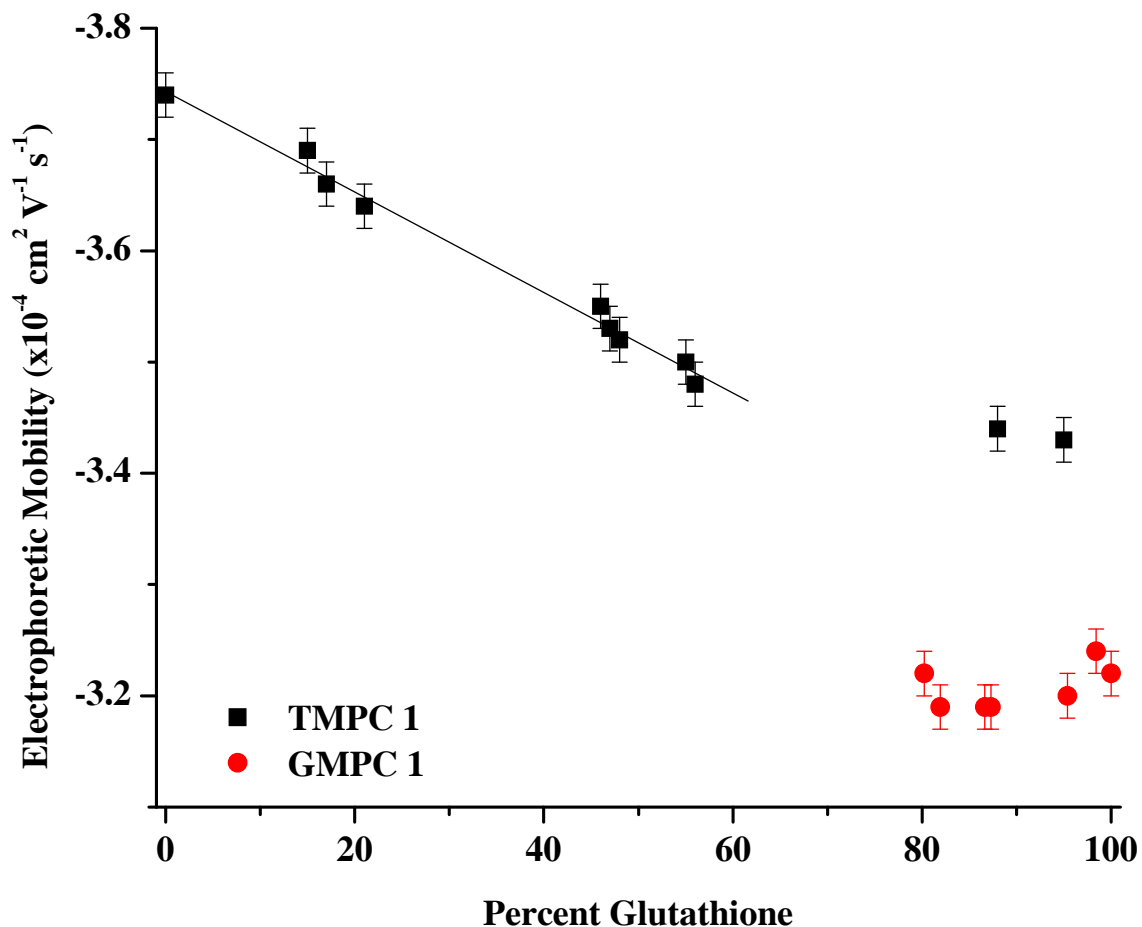


Figure 2.2. Evaluation of μ_{EP} of MPCs as glutathione concentration was increased in the monolayer. **Black**-The mobility of TMPC 1 place-exchanged with glutathione decreases linearly up to ~60% glutathione. **Red**-The electrophoretic mobility of the reverse place exchange of GMPC 1 with tiopronin remains constant at high concentrations of glutathione. The y-axis has been inverted for clarity.

2.3.3 Hydrodynamic radius and effective surface charge of MPCs

The electrophoretic mobility of place-exchanged MPCs was calculated using equations 1 and 2. However, these equations do not readily lend themselves to understanding the physical properties of MPCs that result in the observed trends in μ_{EP} . The relationship between physical attributes and the electrophoretic mobility of MPCs is defined by equation 2.3.

$$\mu_{EP} = \frac{Ze}{6\pi\eta r_H} \quad (2.3)$$

Where Z is the average effective surface charge of a MPC, e is the electronic charge (1.61×10^{-19} C), η is the solution viscosity ($0.01 \text{ g cm}^{-1} \text{ s}^{-1}$), and r_H is the average hydrodynamic radius of a MPC.⁶⁹ All constants aside, it becomes apparent that the effective surface charge and the hydrodynamic radius are the major factors that determine the electrophoretic mobility of a MPC. If the surface charge were to increase, the magnitude of μ_{EP} would increase and vice versa. Likewise, an increase in the hydrodynamic radius would result in a decrease in μ_{EP} . This is complicated by that fact that Z and r_H of MPCs are inversely co-dependent. For example, an increase in core size increases r_H , which in turn decreases μ_{EP} . However, an increase in core size also increases the number of protecting molecules on the nanoparticle surface which contribute to Z . An increase in the number of protecting molecules increases Z , which in turn increases μ_{EP} . Therefore, it is challenging to know from equation 2.3 whether Z or r_H is the dominant factor that governs the electrophoretic mobility of MPCs.

The asymptotic decrease in electrophoretic mobility as the percent glutathione of the protecting monolayer increases as shown in Figure 2.2 can be explained as a significant change in the overall hydrodynamic radius of the MPCs. The length of

tiopronin, from thiol to carboxylic acid is ~ 7.7 Å, while glutathione has two branches from thiol to terminating carboxylic acids; the longest of which is ~ 12.2 Å according to bond lengths calculated from ChemDraw. From equation 2.3, it follows that as r_H is increased, the electrophoretic mobility of the MPC decreases. Place-exchange of glutathione onto TMPCs replaces the shorter tiopronin for the longer glutathione, increasing the average hydrodynamic radius and decreasing μ_{EP} in linear fashion up to $\sim 60\%$ (Figure 2.2, black). At high percentages of glutathione (Figure 2.2, red), remaining tiopronin ligands do not contribute to the hydrodynamic radius as they are buried in the new monolayer, and the electrophoretic mobility of the MPCs stops decreasing and levels off.

The effective surface charge, Z , of MPCs can be calculated using equation 2.3, by estimating r_H as the radius of the gold core plus the length of the protecting ligand. The effective surface charge was determined to be $Z = -8.8$, $Z = -9.4$, and $Z = -10.5$ for TMPC 1, TMPC 2, and GMPC from Table 2.1, respectively. It is important to note that the effective surface charges for these MPCs are far lower than the average total number of ionizable carboxylic acid groups available (Table 2.1). This phenomenon has been previously observed for MPCs and is attributed to a screening or stabilization of a significant portion of the deprotonated carboxylic acids by the oppositely charged buffer electrolyte.¹¹

From an effective surface charge point of view, the decrease in electrophoretic mobility as the amount glutathione is increased is initially surprising. One would expect as tiopronin ligands with a single terminating carboxylic acid group were replaced with glutathione with two carboxylic acids per ligand that the effective surface charge would

increase and therefore so would μ_{EP} as a result from equation 2.3. Instead, the opposite trend is observed, the effective surface charge drops from -8.8 to -8.1 as the percentage of glutathione increases from 0% to 96% assuming the hydrodynamic radius is held constant. As described above, there is reason to believe that r_H is not constant and increases as the amount of glutathione increases. This suggests that the change in the hydrodynamic radius of the MPCs is the dominant effect, to the extent that it supersedes the increase in available surface charges as more glutathione is inserted into the protecting monolayer. Clearly, if the effective surface charge, Z , was the dominating factor that governed the electrophoretic mobility of these MPCs, an increase in the surface charge and electrophoretic mobility would be observed rather than a decrease.

2.3.4 Electrophoretic Mobility of MUA exchanged TMPCs

While tiopronin and glutathione are very similar in structure, they have differences in size and potential charge. Glutathione is longer and has two ionizable carboxylic acids compared to the shorter tiopronin. Therefore, it is challenging to confidently assign changes in electrophoretic mobility solely due to hydrodynamic radius or effective surface charge. To confirm the results, tiopronin MPCs (TMPC 2) were place-exchanged with 11-mercaptoundecanoic acid (MUA), a longer ligand ($\sim 16.8 \text{ \AA}$) with only one terminating carboxylic acid as listed in Table 2.2. Similar to the previous exchange with glutathione, the electrophoretic mobility decreased from $-3.85 \pm 0.02 \times 10^{-4}$ to $-3.21 \pm 0.02 \times 10^{-4} \text{ cm}^2 \text{ V}^{-1} \text{ s}^{-1}$ as the percentage of MUA was increased from 0% to 65% respectively. In this case, tiopronin and MUA are both terminated with only one

carboxylic acid; however, MUA is approximately twice as long, increasing the hydrodynamic radius without changing the number of available surface charges.

Unlike the place-exchange with glutathione, the exchanged MUA peak did not shift migration times with increasing amounts of MUA. Instead, the migration time of the MUA exchanged MPC peak (Figure 2.3, MUA) was fairly constant across the range of place-exchange, but peak height increased with increasing amounts of MUA. Likewise, the peak height of the original tiopronin MPC peaks (Figure 2.3, T1, T2, T3) decreased as the percentage of MUA was increased. As shown in Figure 2.3, the major tiopronin peaks (T1, T2) appear to slowly decrease in intensity though at different rates. The peak T1 was the most prominent tiopronin peak until the 10% MUA where T2 became slightly higher. By 16% MUA, T1 was a shoulder on T2 and at 44% MUA the intensity of T1 and T2 had decreased to about the same intensity before disappearing altogether at 65% MUA. The third, smaller tiopronin peak (T3) seemed to decrease as well, but after 5% exchange became buried under the growing MUA peak and so was not used in data analysis. The change in the dominant peak as MUA is exchanged onto the TMPCs, as shown in Figure 2.3, could classically be described the spectrophotometric titration shown in equation 2.4.



Where Au_xTiop_y are the un-exchanged TMPCs (T1, T2, and T3), MUA is the titrant and $\text{Au}_x\text{Tiop}_{y-z}\text{MUA}_z$ represents the newly formed MUA-exchanged MPCs. As equation 2.4 suggests, as Au_xTiop_y is titrated with MUA, its absorbance would decrease, while the absorbance of $\text{Au}_x\text{Tiop}_{y-z}\text{MUA}_z$ would increase. As shown in Figure 2.4, the absorbance T1 and T2 TMPC peaks decrease linearly while the absorbance of the MUA exchanged

TMPCs increased in similar fashion as a function of mole fraction of MUA. The slopes of the best fit lines were determined to be 0.054, -0.079, and -0.051 for MUA, T1, and T2 respectively. The differences in the slope for T1 and T2 also indicate that T1 decreased faster than T2 as the amount of MUA in the protecting monolayer increased. This would suggest that the population of MPC sizes that make up T1 are preferentially exchanged with MUA over T2 and T3 MPCs at low concentrations of MUA (below 16%). Since, as stated previously, these MPCs migrate through the capillary in order of largest to smallest, the MPCs in the T1 peak would represent the smallest sizes of MPCs. This phenomenon has been reported previously by Guo *et al.* who demonstrated that exchange reactions are much slower on larger MPCs due to the presence of larger terrace-like surface atom content when compared to smaller MPCs.⁷⁰

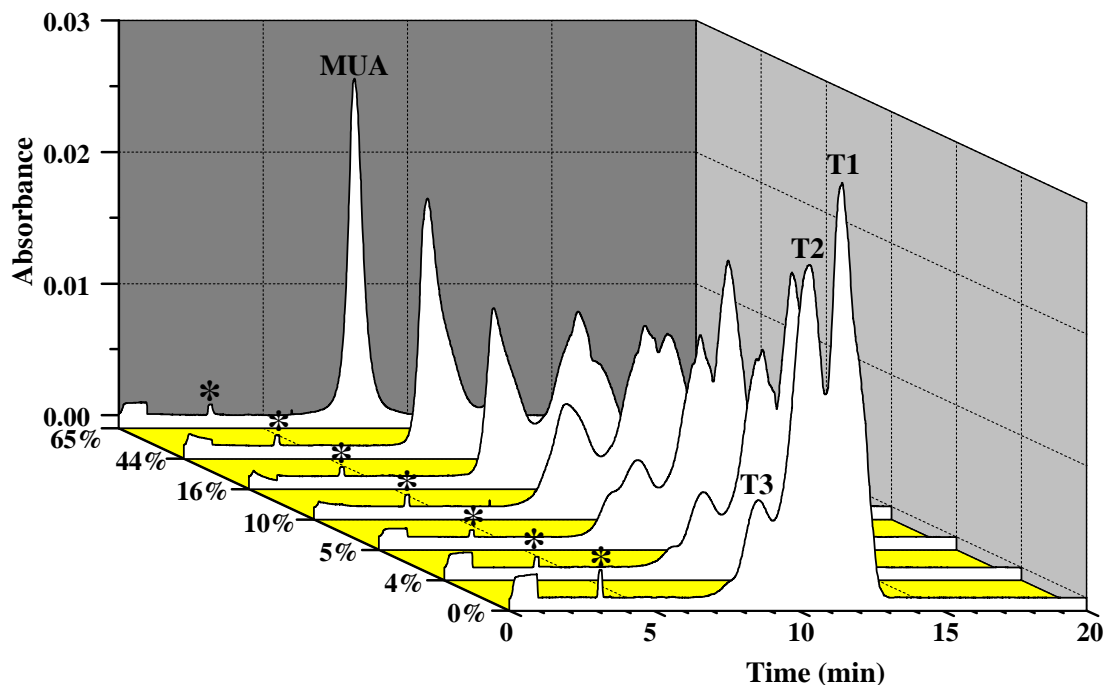


Figure 2.3. Electropherograms of TMPC 2 place-exchanged with MUA from 0-65%. **T1,T2,T3**-electropherogram peaks from TMPC 2 that consist of more narrow size populations of MPCs with electrophoretic mobilities of -3.37 , -3.96 , $-3.85 \pm 0.02 \times 10^{-4} \text{ cm}^2 \text{ V}^{-1} \text{ s}^{-1}$ respectively. Peaks decrease in intensity as more MUA is exchanged onto the MPC. **MUA**-electropherogram peak of MUA exchanged MPCs with electrophoretic mobility of $-3.21 \pm 0.02 \times 10^{-4} \text{ cm}^2 \text{ V}^{-1} \text{ s}^{-1}$. Peak increases in intensity with increasing exchange of MUA. Absorbance values have been normalized to correct for variations in sample concentration. Asterix indicate the neutral marker, mesityl oxide.

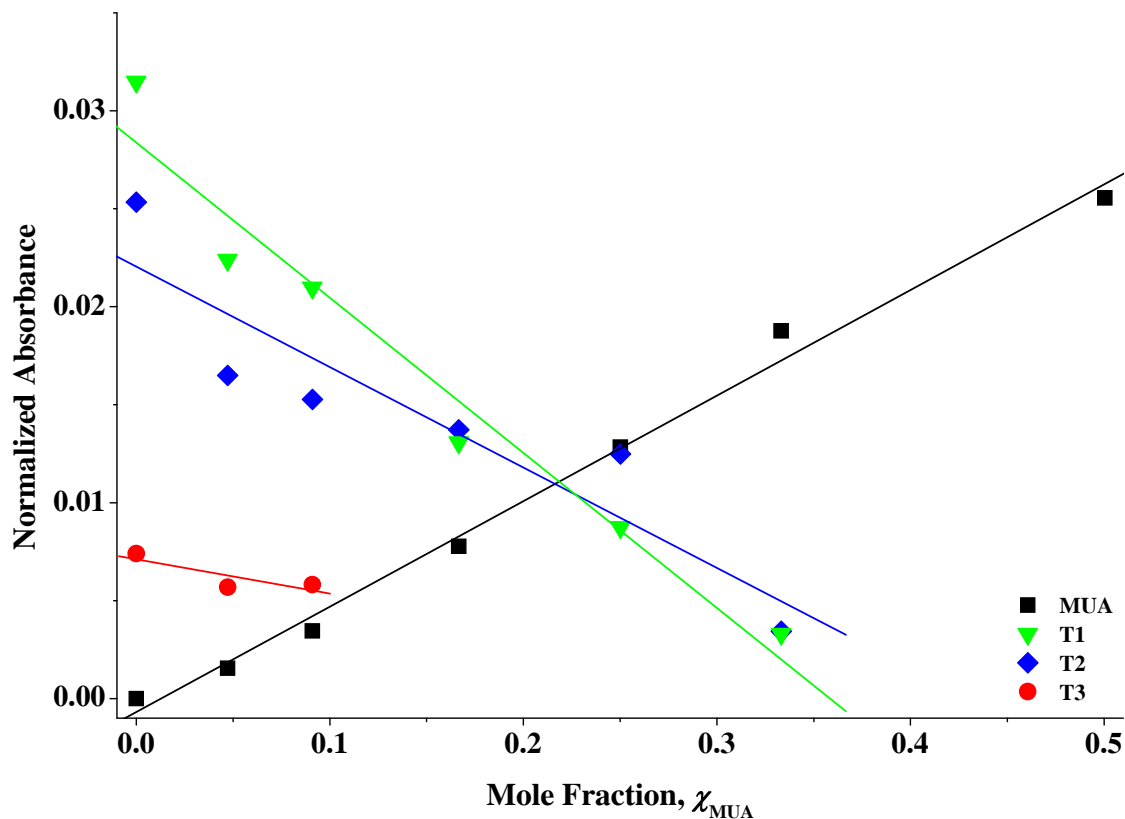


Figure 2.4. Normalized absorbance of peak maxima from Figure 2.3 as a function of mole fraction MUA (χ_{MUA}). **T1(Green Triangle)**-TMPC 2 MPCs of smallest sizes, $m = -0.079$ $R^2 = 0.98$. **T2(Blue Diamond)**- TMPC 2 MPCs of larger sizes, $m = -0.051$ $R^2 = 0.92$. **T3(Red Circle)**- TMPC 2 MPCs of largest sizes. **MUA(Black Square)**- TMPC 2 MPCs exchanged with MUA, $m = 0.054$ $R^2 = 0.99$.

2.4 Conclusions

In summary, capillary electrophoresis has been used to investigate the electrophoretic properties of monolayer protected clusters by carefully controlling the monolayer composition. As longer chain protecting ligands are exchanged into the monolayer, the electrophoretic mobility of the MPCs decrease due to an increase in the hydrodynamic radius. Interestingly, if at the same time the number of charge contributing groups is increased, as is the case with glutathione on TMPCs, the electrophoretic mobility still decreases. The effective surface charge, therefore, appears to have significantly less effect on the electrophoretic mobility of place-exchanged MPCs than the hydrodynamic radius. This leads to the conclusion that the ionic shielding of the effective surface charge on the nanoparticle is highly efficient, and thus the ability to modify the MPC charge is more limited than modification of MPC hydrodynamic size. Furthermore, there is evidence to suggest that place-exchange reactions do not occur similarly across the range of MPC sizes. Rather, as evidenced when MUA was exchanged onto TMPCs, the incoming exchange ligands preferentially exchange with the smaller MPCs first.

CHAPTER III

OPTICAL CHARACTERIZATION OF CONTINUOUS FREE-FLOW ELECTROPHORETICALLY SIZE SEPARATED TIOPRONIN MONOLAYER PROTECTED CLUSTERS

3.1 Introduction

Electrophoresis is among the most promising and least studied techniques for separation of polydisperse metal nanoparticles into monodisperse fractions. Using electrophoretic techniques, metal nanoparticles are separated according to properties such as electrophoretic mobility, effective surface charge and charge-to-size ratio. Capillary and gel electrophoresis, CE and GE respectively, have been shown to effectively separate samples of polydisperse nanoparticles on a small scale.^{11, 31, 51, 52, 71} The major disadvantage of electrophoretic techniques to separate polydisperse metal nanoparticles has been the lack of a preparative scale electrophoretic technique. Recently, however, Peterson *et al.* used continuous free-flow electrophoresis (CFFE) to separate metal nanoparticles on a preparative scale, producing milligram quantities of greater monodispersity.⁵⁷

Members of the Cliffel group are particularly interested in applications of metal nanoparticles involving peptide functionalized surfaces for use as immunosensor calibrants.^{28, 29} Electrophoresis is a common step in the purification process of peptides and so it should follow that we can separate peptide modified nanoparticles, but to our knowledge the study of the electrophoretic properties of peptide modified nanoparticles has never been attempted. This area of interest could be expanded to determine the

electrophoretic properties of metal nanoparticles linked in pairs or linked by protein in addition to peptide modified nanoparticles. Also, improving the monodispersity of our nanoparticles could lead to the selection of specific sizes of nanoparticles for use in practical applications such as selecting specific sizes of nanoparticles for coupling reactions, or for peptide functionalized nanoparticles.

We propose that further investigation of these questions will lead to improved separation of polydisperse samples into increasingly more monodisperse fractions in large quantities (milligrams). With a better understanding of these properties, the dispersity of fractionated nanoparticles could be reduced to the atomic level, differentiating between two monodisperse samples in terms of only a few atoms. This is beneficial to the study of not only the size dependent electrophoretic properties, but all size dependent properties of this material as more monodisperse sizes become more readily available. In addition, this study will add to the fundamental understanding of nano-materials, providing a backbone for future investigation. Finally, development of electrophoretic methods for separation of metal nanoparticles opens the door to the possibility of applying these electrophoretic techniques to the separation of other types of nano-materials such as semiconductor nanocrystals, quantum dots, polymer nanoparticles, and dendrimers.

In this chapter, we present the separation of polydisperse tiopronin MPCs into more monodisperse fractions *via* CFFE in comparison to previous work by Peterson *et al.*⁵⁷ The properties of these fractions were investigated using UV/Vis spectroscopy, near-infrared fluorescence spectroscopy, and capillary electrophoresis techniques.

Determinations as to monodispersity and optical properties of the fractions are presented here.

3.2 *Experimental Methods*

3.2.1 *Reagents and Chemicals*

$\text{HAuCl}_4 \cdot 3\text{H}_2\text{O}$ was synthesized according to literature.⁶⁷ N-(2-mercaptopropionyl) glycine (tiopronin, 99%) was purchased from Sigma, and 11-bromo-1-undecene (95%), and mesityl oxide (90%) were purchased from Aldrich. Trimethylamine (25 w/w % in MeOH), NaBH_4 (98+%), glutathione (98% reduced), and thioacetic acid (98%) were purchased from Acros, and sodium tetraborate (99.8%), tris (hydroxymethyl) amino methane (Tris), and boric acid were purchased from Fisher. Water was purified in house using a Barnstead NANOpure Diamond system. All other chemicals were reagent grade and used as received.

3.2.2 *MPC Synthesis*

Tiopronin protected gold MPCs (TMPCs) were synthesized from $\text{HAuCl}_4 \cdot 3\text{H}_2\text{O}$ as according to Templeton *et al.*¹ Briefly, approximately 1 g of $\text{HAuCl}_4 \cdot 3\text{H}_2\text{O}$ was dissolved in 100 mL of a 6:1 methanol:acetic acid solution in a 1 L round bottom flask. Tiopronin was then added (1.44 g, 3 equiv.) to give a ruby colored solution, which quickly faded to a milky white/pale yellow solution. The temperature was then lowered to 0 °C by placing the round bottom flask into an ice bath. In a separate beaker, NaBH_4 (1.11 g, 10 equiv.) was dissolved in deionized (DI) water and added over approximately

10 seconds to the cooled round bottom flask to immediately give a black precipitate. Solution was allowed to stir either overnight for larger clusters or for 30 minutes for smaller clusters before evaporation of the organic solvent under vacuum. The remaining aqueous solution was acidified to a pH of 1 with concentrated HCl and dialyzed for ~ 1 week in cellulose ester dialysis tubing (Spectra/Por, 10,000 MW cutoff) changing the water twice daily. The sample was then extracted from the tubing, and filtered through a fine glass frit. The collected black solution was then dried under vacuum to yield a black flaky solid. The synthesis of larger average diameter MPCs was completed as described above with the exception that only 0.2 g (0.5 equiv) of tiopronin was used for 1 gram of $\text{HAuCl}_4 \cdot 3\text{H}_2\text{O}$.

3.2.3 Transmission Electron Microscopy (TEM)

Samples were prepared by dissolving a small amount of TMPCs in 1 mM HCl and diluting the sample until the faint brown color was barely visible. One drop was then placed onto 400 mesh grids coated with ultrathin carbon flim and holey carbon support (Ted Pella, Redding, CA, Product # 01824) and allowed to air dry overnight. TEM images were obtained on a Phillips CM20 electron microscope operating at 200 kV at magnifications of 200Kx and 400Kx. The negatives were developed and digitized in Adobe Photoshop for measurement. Cluster diameters were measured along the major elliptical axis using ImageJ version 1.41 (available at <http://rsbweb.nih.gov/ij/>).

3.2.4 Thermal Gravimetric Analysis (TGA)

Samples were dried under vacuum overnight prior to analysis to remove moisture. TGA was performed with an ISI TGA 1000 system on 5-10 mg of dry sample under N₂ (flow rate of ~60 mL/min) in a platinum pan (Instrument Specialists Inc.). Data was recorded from 20 – 900 °C at a heating flow rate of 20 °C/min. A brittle, gold solid of elemental gold remained after analysis.

3.2.5 Nuclear Magnetic Resonance Spectroscopy (NMR)

For solid samples, approximately 20 mg of sample was weighed into an NMR tube and dissolved in ~ 600 µL of D₂O. Samples in aqueous solution were concentrated and 2-3 drops of D₂O was added. Spectra were obtained on a 400 MHz Bruker NMR collecting at least 40 scans with a d1 delay of 1.5 seconds. A double WATERGATE pulse program was used for water suppression.

3.2.6 Ultraviolet-Visible Spectroscopy (UV-Vis)

UV/Vis spectra were obtained of MPC samples on a Cary 100 Bio UV/vis spectrophotometer in the range of 200-800 nm with a 1 nm resolution in 1 cm plastic cuvettes. Samples were prepared at concentrations around 0.2 mg/mL in DI water.

3.2.7 Near-Infrared Fluorescence

NIRF spectra of fractionated MPCs were obtained on a Fluorolog near-infrared spectrofluorimeter between 600-1600 nm with excitation wavelengths of 400, 450, and 590 nm. Prior to experiment, all fractions were diluted to a concentration of 0.2 mg/mL or 0.1 mg/mL and run on the UV/Vis spectrophotometer to assure that UV absorbance at the excitation wavelengths were < 0.1 to minimize self-absorbance in the fluorescence spectra.

3.2.8 Capillary Electrophoresis

Capillary electrophoresis experiments were conducted on a P/ACE MDQ CE with a UV detector from Beckman-Coulter, courtesy of Professor Michael Stone. Experiments were conducted in a fused silica capillary (50 μm i.d., 362 μm o.d., and 60 cm total length (50 cm to the detection cell). New capillaries were rigorously conditioned prior to initial use by hydrodynamically flushing at 30 psi with DI water (5 min), 1.0 M NaOH (30 min), 0.1 M NaOH (30 min), DI water (50 min), and finally running buffer (30 min). Before each experiment, the capillary was washed with a less rigorous treatment of 0.1 M NaOH, DI water, and running buffer (typically, 20 mM sodium borate, pH = 9.3) for 5 minutes each at 30 psi. The sample solutions were filtered through a 0.2 μm nylon syringe filter and placed into 2 mL glass sample vials. Approximately 1 mg of sample was weighed out and placed in a 2 dram vial and dissolved to a concentration of 1 mg/mL with 20 mM sodium borate buffer (pH = 9.3). 1 μL of a neutral marker solution (990 μL buffer, 10 μL mestiy oxide) was then added for

CE experiments. The MPC samples were injected hydrodynamically (5 psi for 5 s) at the anode and were detected using UV/Vis (214 nm) near the cathode through a window burned through the polyimide coating of the capillary. All experiments were run under a constant voltage of 30 kV with the capillary cooled to 25 °C.

3.2.9 Continuous Free-Flow Electrophoresis (CFFE)

Initial experiments were conducted on a prototype commercial CFFE instrument made by R & S Technologies on location at the University of Cincinnati with a Bertan 105-01R power supply in constant voltage mode at 600 V (80.9 mA) in 8.9 mM tris-borate buffer pH 8.2, 102 μ S/cm. A twin of this prototype was acquired from Dr. Apryll Stalcup at the University of Cincinnati. Prior to use, instrument was repaired and refurbished in house. MPCs were separated using a Bertan 105-02R power supply from Spellman High Voltage in constant voltage mode at 500 V (20.8 mA) in 7.3 mM tris-borate buffer (pH 8.8) with a conductivity of 48.0 μ S/cm. Fractions were collected in 48 separate 9½ dram vials. Fractions of interest were dialyzed in 10,000 MW dialysis tubing for 3 days to remove buffer components and were then dried under vacuum. The weight of MPCs in each fraction was then recorded.

3.3 Results and Discussion

3.3.1 Synthesis and characterization of MPCs

Tiopronin protected MPCs were synthesized as described in the experimental methods section and characterized *via* NMR, TGA, TEM and UV-vis spectroscopy to determine purity and composition of the MPCs. For the experiments described here, three separate batches of tiopronin MPCs (TMPCs) were prepared with diameters of 2.1 ± 0.7 , 2.5 ± 0.6 , and 2.9 ± 0.9 nm, respectively (Table 3.1). It is important to note that the MPCs produced by this synthesis were not a single size, but rather a range of sizes typically around 1-5 nm. As a result, the data in Table 3.1 represents the *average* composition of MPCs in each batch.

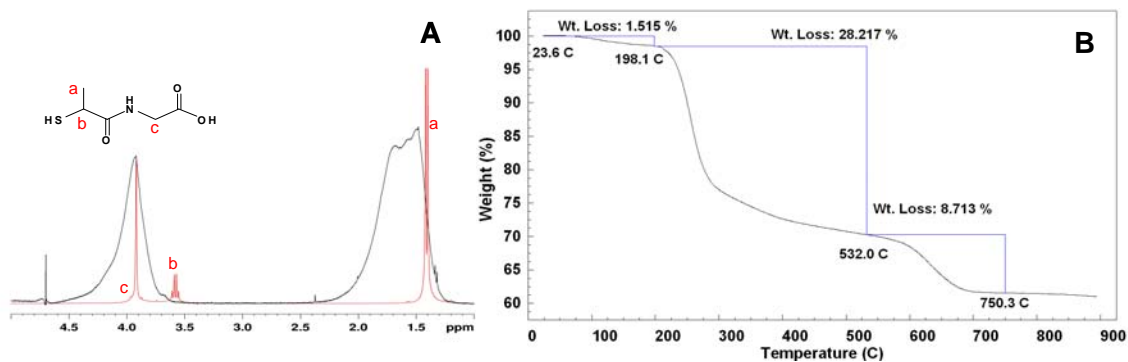
Table 3.1. Nanoparticle composition of synthesized MPCs

Batch ID	Ligand type	Composition d ^a , %O ^b	Average molecular formula
TMPC 3	Tiopronin	2.1±0.7, 37%	Au ₁₇₉ TiO ₁₁₆
TMPC 4	Tiopronin	2.5±0.6, 34%	Au ₃₀₈ TiO ₁₇₅
TMPC 5	Tiopronin	2.9±0.9, 22%	Au ₄₆₈ TiO ₁₃₉

^a Diameter in nm with standard deviation of gold core as measured from TEM. ^b Percent organic from TGA data.

Figure 3.1 depicts the characterization results for the TMPC 3 batch described in Table 3.1. NMR of the tiopronin clusters indicates the purity of the sample. The broad spectrum (black) in Figure 3.1A represents the NMR spectrum of tiopronin ligands bound to the nanoparticle, while the narrow spectrum (red) is an overlay of free tiopronin in solution. Broadening of the methyl (a) and methylene (c) resonances when tiopronin is attached to the clusters has been attributed to exceedingly short T₂ relaxation times

arising from a distribution of chemical shifts associated with the variety of shapes, sizes, and defects of the gold cores present in the sample.⁷² The presence of any narrow resonances from pure tiopronin (red) would indicate the presence of unbound tiopronin in the sample. As can be seen in Figure 3.1A the MPC spectrum (black) has no narrow tiopronin resonances, indicating that the sample was clean of starting material impurities. Determination of the average cluster size and molecular formula was achieved using TGA of tiopronin MPCs (Figure 3.1B) to determine the percent organic of the MPCs, while TEM (Figure 3.1C) was used to visually measure the core diameters of the MPCs. The UV-vis spectra (Figure 3.1D) shows no surface plasmon band (SP band) at ~520nm, which would indicate smaller sized MPCs overall. MPC batches, TMPC 4 and TMPC 5 were similarly characterized; however, a small SP Band was present in the UV-vis spectrum of TMPC 5.



Au₁₇₉Tiopronin₇₉

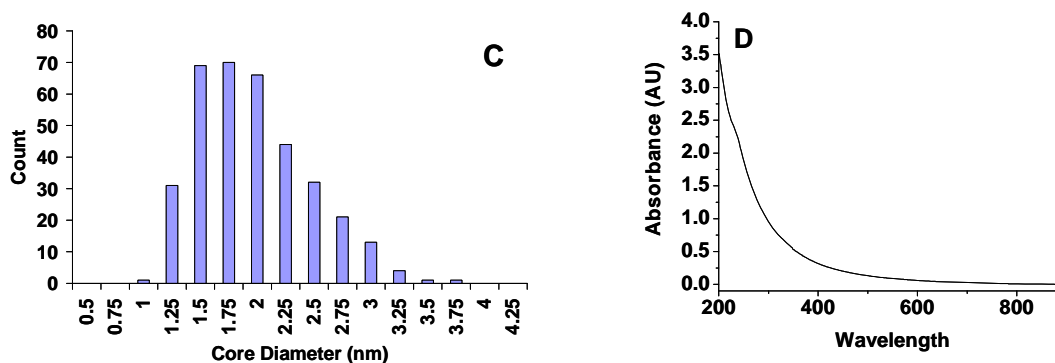


Figure 3.1 Characterization data for TMPC 3. **(A)** Broad NMR spectrum of MPC bound tiopronin (Black) overlaid with the narrow spectrum of free tiopronin ligand (Red). The absence of narrow peaks in the NMR spectrum of the TMPCs (Black) indicate the sample is clean. **(B)** TGA of tiopronin MPCs, 1.52% water, 36.93% organic tiopronin ligand. **(C)** TEM histogram of MPCs, average diameter 2.1 ± 0.7 nm. **(D)** UV-vis spectrum of MPCs with no surface plasmon band present.

3.3.2 *Continuous Free-Flow Electrophoresis of Tiopronin MPCs*

Two CFFE separations of TMPCs were performed. The first, using the twin to our instrument at University of Cincinnati to separate TMPC 3, and the second using our CFFE apparatus to separate a 1:1 mixture of TMPC 4 and TMPC 5. A mixture of these TMPC batches was used in the second experiment to increase the range of polydispersity of the sample to be separated. The mixture of these two samples, large and small, allowed for a larger range of separation. Like TMPC 3, TMPC 4 had no SP band in the UV-vis spectrum of the unfractionated nanoparticles and thus was comprised mostly of small nanoparticles. TMPC 5 on the other hand, had been synthesized to make larger particles that exhibited a SP Band. CFFE of these samples separated TMPC 3 nanoparticles into 25 fractions, while separation of TMPC 4/TMPC 5 resulted in 35 fractions. Fractions from both experiments were characterized by UV/Vis, and NIRF. Prior to characterization, samples were processed as described in the experimental methods section to remove buffer components and adjust sample concentrations to 0.2 mg/mL (TMPC 3) or 0.1 mg/mL (TMPC 4/TMPC 5) for each fraction.

3.3.3 *UV-visible absorbance of CFFE fractions*

UV-vis spectroscopy was used to determine if a SP band at ~520 nm was present in any fraction. This would determine which fractions have the larger MPC cores and which would not. For the separation of TMPC 3, no SP band was visible in any fraction as can be seen in Figure 3.2A. This indicated that this batch of nanoparticles has an average size that is too small to exhibit the SP band; indeed, the UV-vis spectrum of the unfractionated sample also does not have a SP band (Figure 3.1D). For the separation of

TMPC 4/TMPC 5, a SP band was apparent in the later fractions, (F14-F35) as shown in Figure 3.2C but not in the earliest fractions (F1-F13, Figure 3.2 B). Additionally, the intensity of the UV-vis absorbance at the wavelengths of fluorescence excitation was extracted for comparison to the NIR fluorescence data. As shown in Figure 3.3, there is a general trend of increasing absorbance intensity across the range of CFFE fractions for each excitation wavelength. It is important to note that each fraction has been diluted to the same concentration in mg/mL and so changes in absorbance from fraction to fraction are do not arise from varying concentrations, but from differences in the nanoparticle size distribution in each fraction.

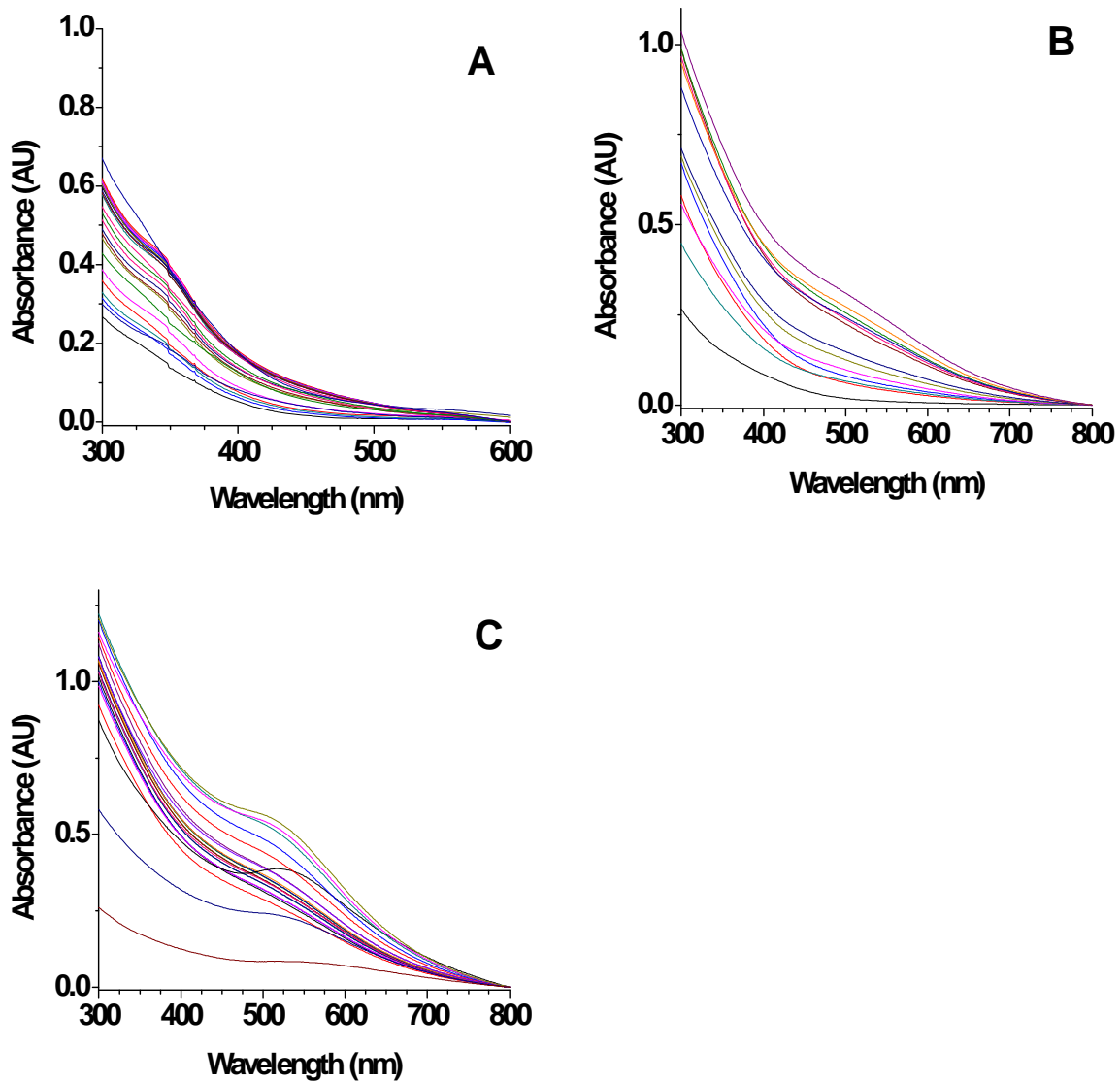


Figure 3.2 UV-visible spectra of CFFE fractions. (A) Fractions from separation of TMPC 3 at 0.1 mg/mL concentrations indicating no SP band. (B) Fractions 1-13 from separation of TMPC 4/TMPC 5 at 0.1 mg/mL concentrations with no SP band. (C) Fractions 14-35 from separation of TMPC 4/TMPC 5 at 0.1 mg/mL concentrations depicting a SP band.

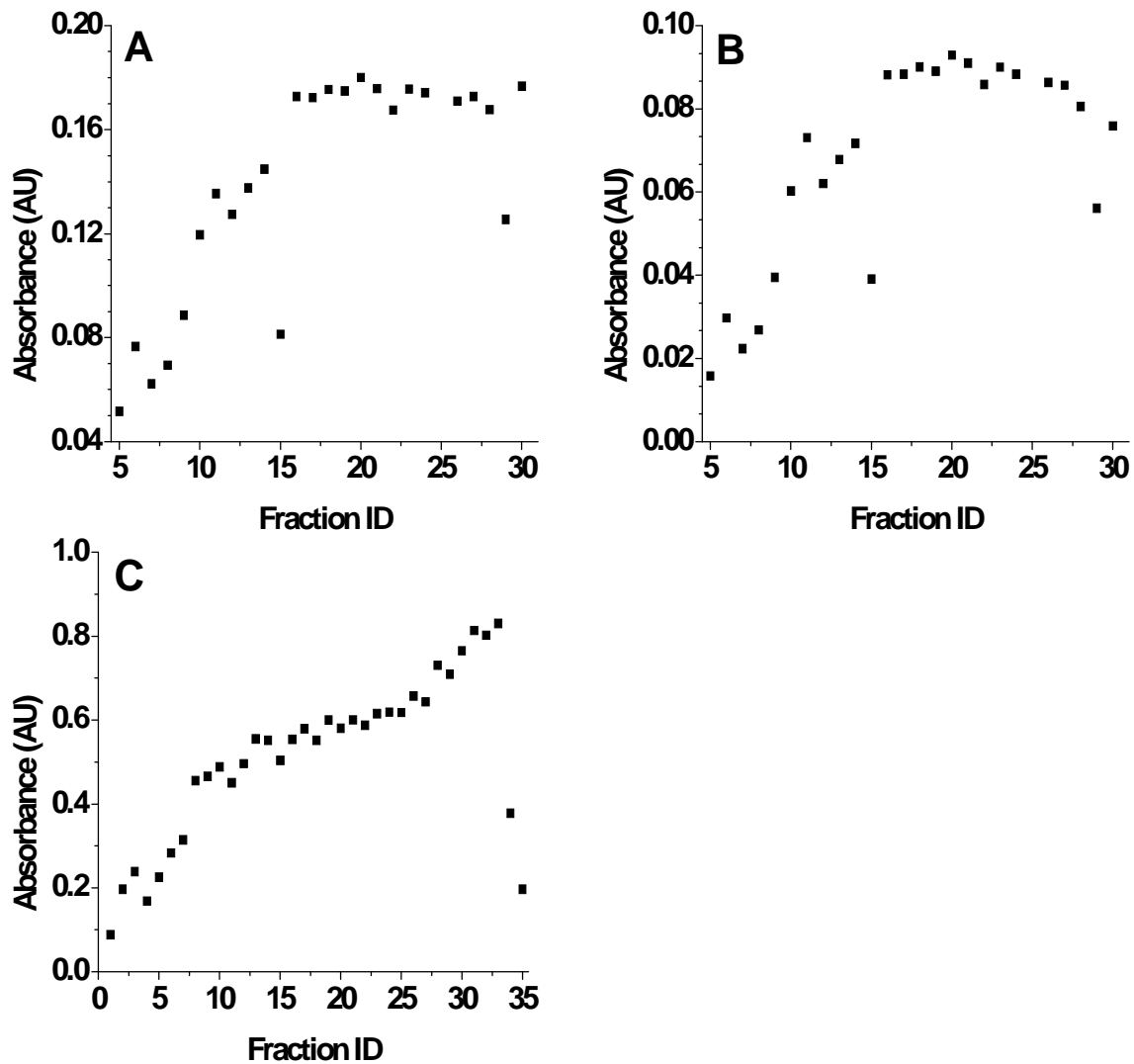


Figure 3.3. Plots of absorbance intensity vs. fraction ID at fluorescence excitation wavelengths. (A) TMPC 3 at 400 nm indicating a trend in increasing intensity from fraction 5 to fraction 30. (B) TMPC 3 at 450 nm indicating a trend in increasing intensity from fraction 5 to fraction 30. (C) TMPC 4/TMPC 5 at 400 nm indicating a trend in increasing intensity from fraction 1 to fraction 35.

3.3.4 Near Infrared Fluorescence of CFFE fractions

More promising results arose from the near-infrared fluorescence of the MPC fractions. Figure 3.4 shows the baseline corrected data of the NIR fluorescence of TMPC fractions when excited at 400 and 450 nm for the TMPC 3 separation (Figure 3.4A, B) and excited at 400 nm for the TMPC 4/TMPC 5 separation. The fluorescence intensity of the TMPC 4/TMPC 5 fractions at 450 nm were too low for analysis and so are not shown. For both TMPC 3 and TMPC 4/TMPC 5 fractions, the emission peaked at 922 nm for 400 nm excitation and at 907 nm for 450 nm excitation. A plot of the peak intensity *versus* fraction number is provided for each plot (Figure 3.4, insets). For the TMPC 3 fractions (Figure 3.4A and B, insets) a noticeable trend in increasing fluorescent intensity with increasing fraction number was observed, similar to the UV-vis absorbance trend at their respective excitation wavelengths (Figure 3.3 A, B). For the TMPC 4/TMPC 5 fractions (Figure 3.4C inset), the fluorescent intensity remained relatively constant across the range of fractions. A plot of fluorescence emission/absorbance versus fraction number leads to a trend shown in Figure 3.5, which indicates that the earlier fractions have a higher quantum yield than the later fractions in each experiment. This would suggest that the earlier fractions consist of smaller MPCs whose characteristics are less like bulk gold and more molecular in nature, whereas the later fractions consist of MPCs that have more of a bulk characteristic to them. This fits well with electrophoretic arguments that the smaller MPCs will have a higher charge:size ratio and thus migrate faster and farther through the electric field causing earlier fractions to have the smaller MPCs, while the slower moving and hence larger MPCs would be in the later fractions.

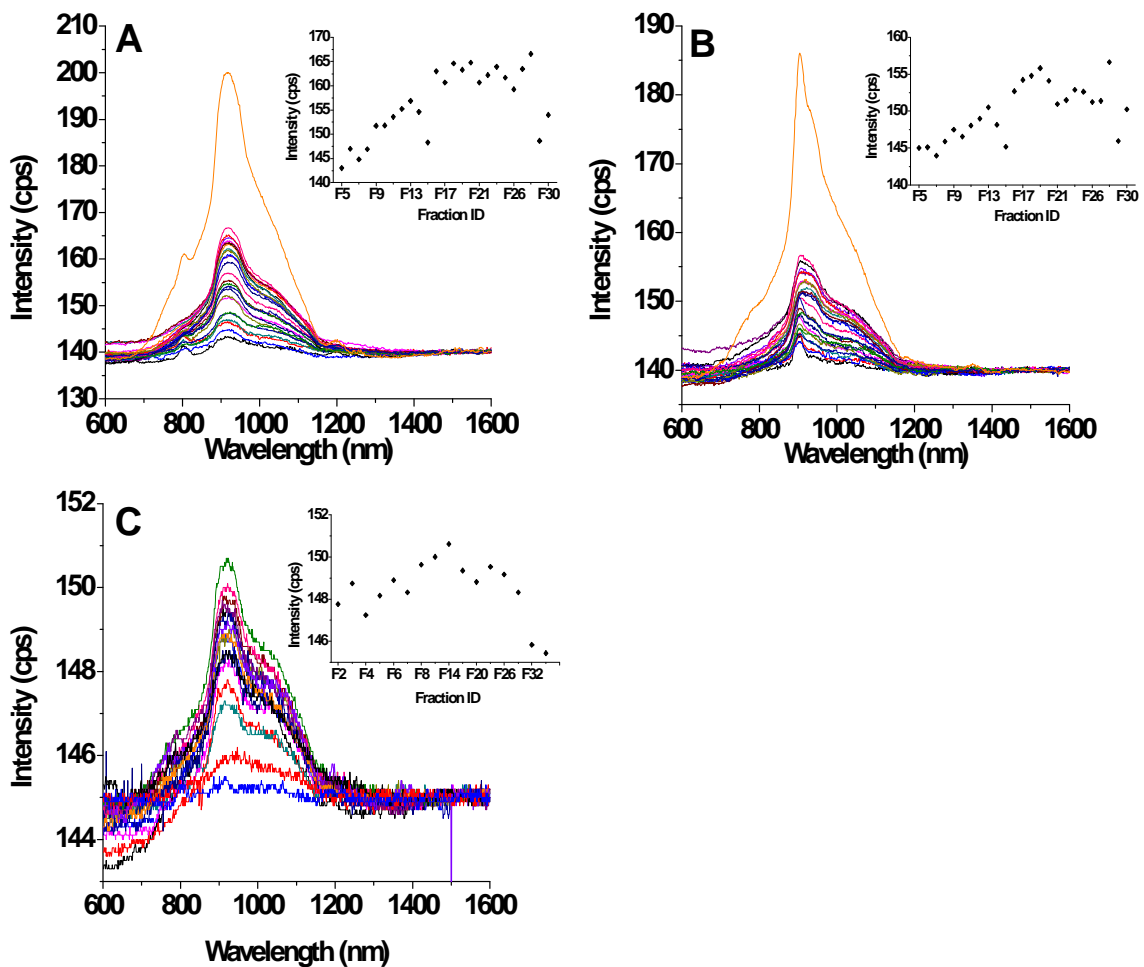


Figure 3.4. (A) NIR fluorescence of TMPC 3 fractions at 400 nm excitation wavelength. (Inset) Plot of peak intensity vs. fraction ID. (B) NIR Fluorescence of TMPC 3 fractions at 450 nm excitation wavelength. (Inset) Plot of peak intensity vs. fraction ID. (C) NIR Fluorescence of TMPC 4/TMPC 5 fractions at 400 nm excitation wavelength. (Inset) Plot of peak intensity vs. fraction ID.

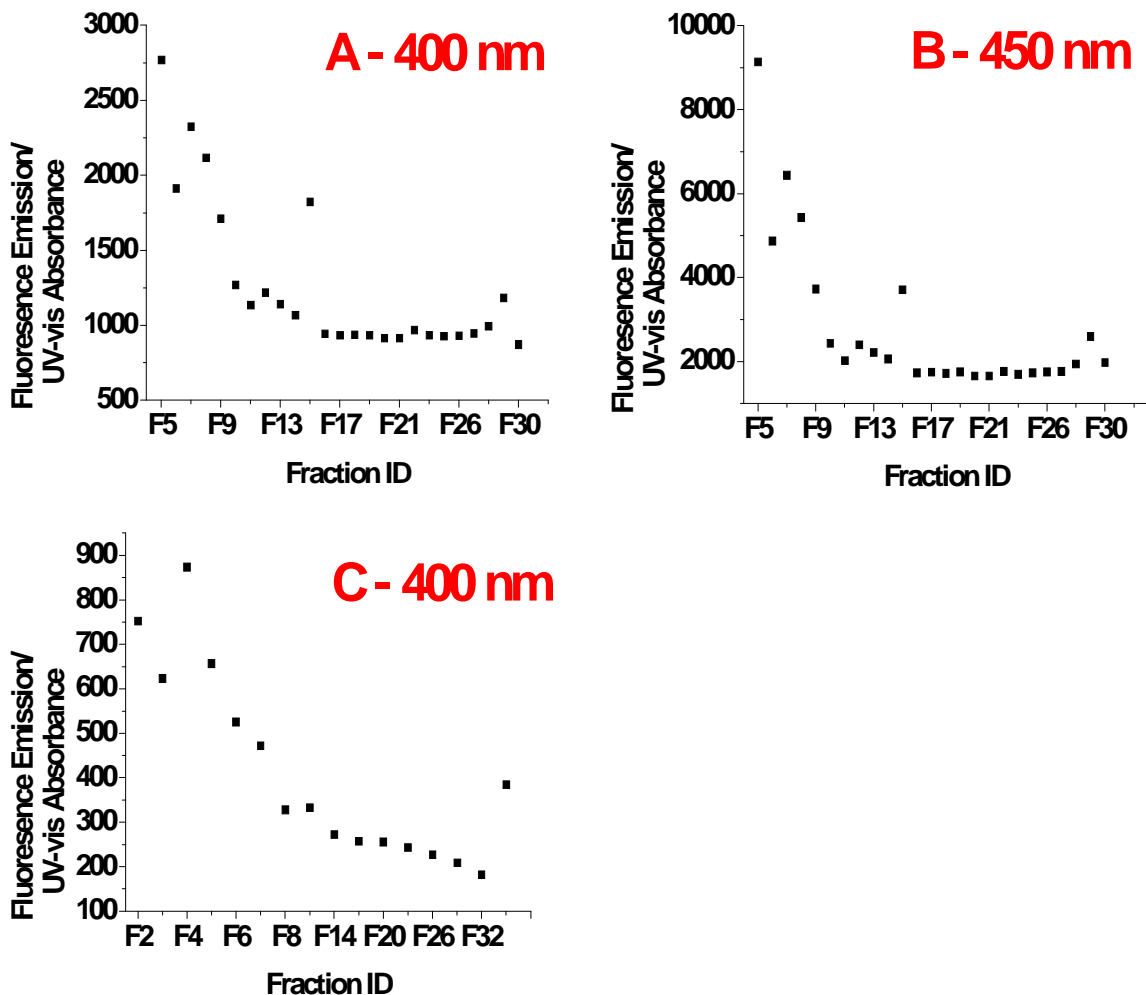


Figure 3.5 (A) Plot of fluorescence emission/UV-vis absorbance vs. fraction id for TMPC 3 fractions at 400 nm excitation, indicating higher fluorescence in the earlier fractions. (B) Plot of fluorescence emission/UV-vis absorbance vs. fraction id for TMPC 3 at 450 nm excitation, indicating higher fluorescence in the earlier fractions. (C) Plot of fluorescence emission/UV-vis absorbance vs. fraction id for TMPC 4/TMPC 5 fractions at 400 nm excitation, indicating higher fluorescence in the earlier fractions.

3.3.5 Using CE to Characterize CFFE Fractions

Capillary electrophoresis was investigated as a technique for rapidly characterizing CFFE fractions of TMPCs. Fractions that have been separated by CFFE are in a buffered solution that is ideal for CE. These fractions were injected as is onto a capillary and analyzed by CE, looking for differences between fractions, without the need to concentrate and dialyze each fraction. Figure 3.6 displays the CE data for every 5th fraction from a separation of the TMPC 3 nanoparticles. Each trace shows a set of three peaks, with similar electrophoretic mobilities from fraction to fraction, but with significant differences in peak intensity. Since the concentrations are not constant from fraction to fraction the peak intensity of each individual trace cannot be said to indicate any differences in size, however, the apparent change in relative peak intensity between peak 1 and peak 2 in each trace is an indication of size fractionation between fractions. As can be seen in Figure 3.6, peak 1 (P1) increases relative to peak 2 (P2) from fraction 5 to fraction 30. A plot of peak 1/peak 2 intensity versus fraction ID (Figure 3.6I) shows a linear change of the dominant peak from peak 2 to peak 1. In order to remain consistent with the migration order expected in CFFE experiments, a change in the dominant peak from peak 2 to peak 1 in Figure 3.6 would indicate a change in core size from smallest to largest from fraction 5 to fraction 30.

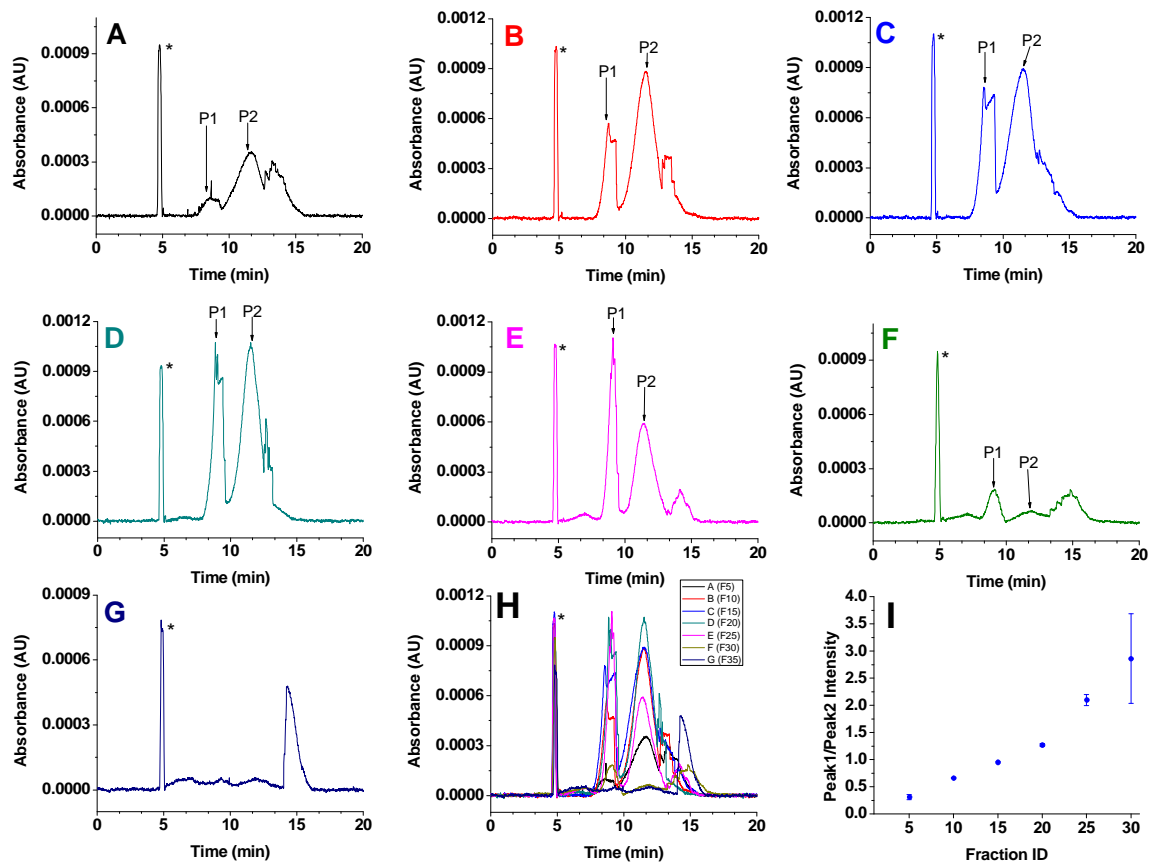


Figure 3.6. CE analysis of TMPC 3 fractionated by CFFE. (A) fraction 5, (B) fraction 10, (C) fraction 15, (D) fraction 20, (E) fraction 25, (F) fraction 30, (G) fraction 35, and (H) overlay of fractions. Note that from fraction to fraction peak 1 increases while peak 2 decreases relative to each other. (I) Plot of peak1/peak2 vs. fraction id indicating an increasing trend in the change from peak 1 to peak 2. (*) neutral marker

3.4 Conclusions

Tiopronin protected clusters have been successfully separated *via* continuous free-flow electrophoresis. UV/Vis and NIRF data indicate that the earlier fractions consist of smaller clusters that exhibit higher quantum efficiency than the later fractions, which consisting of larger clusters. Also, CE analysis of CFFE fractionated TMPCs appears to be a useful technique for rapid characterization of particle distributions across fractions. Furthermore, CE analysis is also in agreement with other characterization techniques, with smaller clusters in earlier fractions and larger clusters in the later fractions.

APPENDIX

CONTINUOUS FREE-FLOW ELECTROPHORESIS OPERATION MANUAL

A1 Rationale

The purpose of this appendix is to provide the reader with a standard operating procedure of the R&S CFFE instrumentation. This appendix should be used as a general guide for understanding the basic principles of CFFE as well as a source for operation suggestions, calibrations, and maintenance requirements.

A2 Instrument History

The Continuous Free-Flow Electrophoresis instrument here at Vanderbilt University was one of several prototype instruments designed by R&S Technology Inc. that were gifted to Dr. Apryll Stalcup from the Department of Chemistry at the University of Cincinnati. Through collaboration with Dr. Stalcup and her group, the Cliffel lab here at Vanderbilt acquired one of these prototypes in the spring of 2007. The instrument was vigorously restored to working condition in the summer of 2007 and tasked to size-separation of monolayer protected clusters.

A3 Instrument Theory

Like all other electrophoretic techniques, analytes are separated in the CFFE by their differences in electrophoretic mobility, or rather differences in analytes ability to migrate through a medium in the presence of an electric field. The electrophoretic mobility of any analyte can be defined in physical terms as shown in equation A1.

$$\mu_{EP} = \frac{Ze}{6\pi\eta r_H} \quad (\text{A1})$$

Where Z is the analytes surface charge, e is the electronic charge (1.61×10^{-19} C), η is the solution viscosity ($0.01 \text{ g cm}^{-1} \text{ s}^{-1}$), and r_H is the analytes hydrodynamic radius. All constants aside, it becomes apparent that the surface charge and the hydrodynamic radius are the major factors that determine an analytes electrophoretic mobility. Therefore, charged analytes migrate towards the oppositely charged electrode according to their charge to size ratio (Z/r_H).

The CFFE electrophoresis chamber is typically a rectangular area filled with buffer into which analytes are injected from the top as shown in Figure A1. CFFE is a continuous technique, so buffer electrolyte and sample are continuously pumped into the chamber. This pumping forces solution through the chamber to the bottom, which has been lined with ports for fraction collection. Separation occurs when an electric field is applied perpendicularly to the flow of buffer. Analytes with a high electrophoretic mobility, μ_{EP} will migrate towards the oppositely charge electrode faster than analytes with a low μ_{EP} and thus separate as diagramed in Figure A1. Without the electric field, no separation would occur and analytes would flow straight down to the bottom of the chamber.

CFFE has several significant differences from other electrophoretic techniques that make it potentially more robust. In CFFE, the separation area is far larger, which allows throughput of more sample. Also, buffer and analyte are pumped through the electrophoresis chamber during the separation, generating a continuous flow of material as opposed to the discrete injections of capillary and gel electrophoresis techniques. Finally, the electric potential is applied perpendicularly to the flow of the analyte, producing a two-dimensional separation.

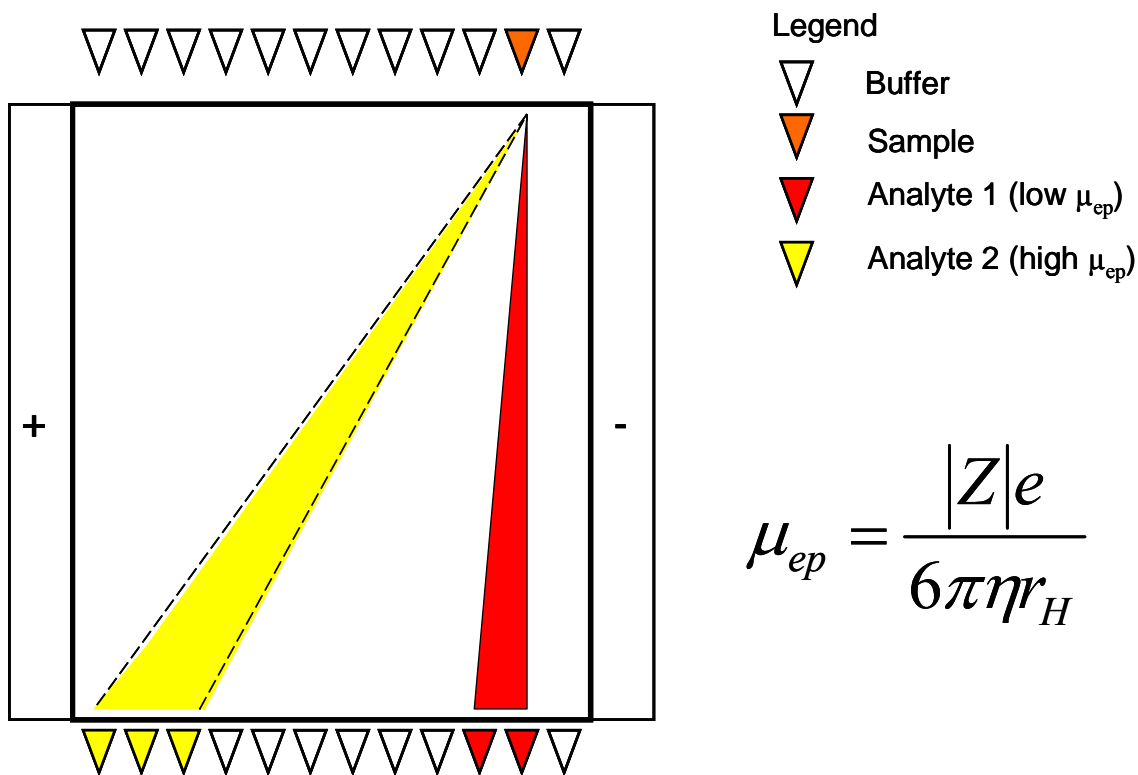


Figure A1. Schematic diagram of a simple CFFE separation. Buffer and sample are added at the top of the chamber (Clear and Orange triangles). Analyte with high μ_{EP} (Yellow) migrates towards the oppositely charged electrode faster and analyte with low μ_{EP} (Red). Analytes are collected at the bottom of the chamber in a fraction collector.

A4 Instrumental Components

The R&S CFFE instrument consists of six basic components; separation chamber, pumps, power supply, fraction collector, cooling system, and outer casing. Successful operation of this instrument requires that the user be aware of problems with any of these components. Here we present a detailed description of each component, their purpose, and suggestions of problems to look for when operating the instrument.

A4.1 Separation Chamber

The separation chamber is diagramed in Figure A2. It consists of a hollow, 14 x 8 x 3 cm rectangular box through which buffer and sample are pumped. Buffer is added through seven ports on the back at the top of the chamber. This spreads out the buffer flow evenly across the width of the separation chamber in order to achieve a laminar flow profile. Additionally, the makeup of the buffer can be varied from port to port for advanced electrophoretic techniques that require a buffer gradient. The sample is injected through one of three ports on the top of the chamber, while the other two remain sealed. Introduction of the sample at different places across the width of the chamber allows greater flexibility of the instrument across a range of sample types. On either side of the main chamber lies an electrode chamber, separated by a thin 0.45 μM nylon membrane. The membrane allows passage of ions and small buffer molecules, but not large bulky analytes. Inside each electrode chamber is a stainless steel mesh electrode approximately 10.5 x 1.5 cm which are attached to the power supply. During operation, buffer is pumped into the bottom and out at the top of the electrode chambers. This is done to prevent ion depletion zones from forming near the electrodes. Typically the

electrode buffer is recycled and reused repeatedly to reduce the amount of buffer consumed by the instrument. From time to time the separation chamber is prone to leaking and should be inspected regularly while running to make sure no significant leaks are present. Most leaks can be stopped with silicone sealant. If the instrument is leaking at the connection of two parts, i.e. where the electrode chambers fit into the separation chamber, tightening of the screws can sometimes stop the leak. Be careful not to over tighten. This instrument is a prototype, and as such, there are no replacement parts should something break. This is the greatest possible difficulty with maintaining the separation chamber. Replacement parts can be fabricated in the machine shop, but at great cost of time and money. Therefore it is recommended to be exceedingly careful with all components of the CFFE separation chamber.

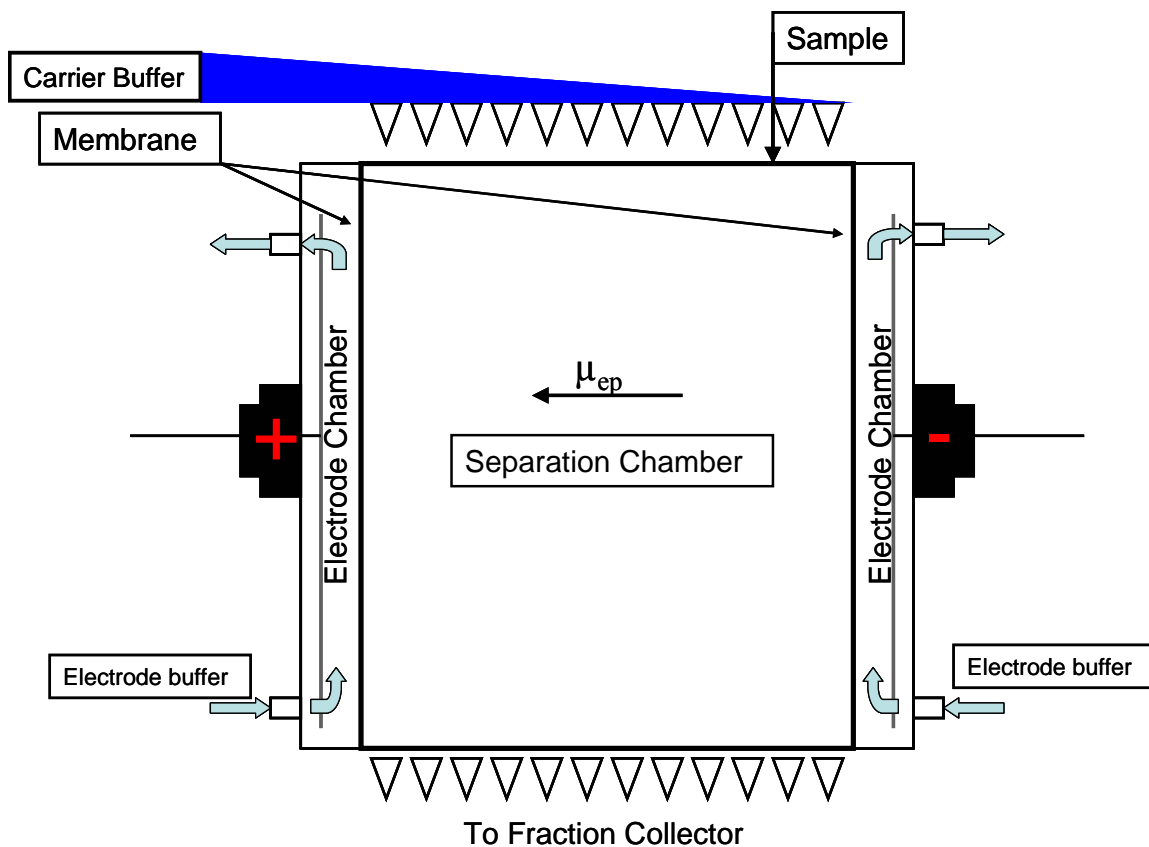


Figure A2. Schematic of CFFE instrument. Sample and buffer are introduced in the top of the chamber, while a voltage is applied perpendicularly across the chamber between two plate electrodes. Electrodes are isolated from the main chamber by 0.45 μm nylon membranes. Fresh buffer is continuously circulated over the electrodes to prevent depletion zones in the buffer.

A4.2 Pumping System

The pumping system is responsible for the flow of all solution inside the CFFE. The system consists of two peristaltic pumps, a sample pump and a buffer pump. The buffer pump controls the flow of buffer through seven chamber inlet lines located on the back of the separation chamber, two electrode inlet lines, and two electrode outlet lines located on the electrode chambers on either side of the separation chamber. The speed of the buffer pump directly controls the flow rate of all solution in the CFFE. The sample pump is solely dedicated to the flow of sample into the top of the separation chamber. This pump also has variable flow rates, however, the sample pump flow rate is always kept significantly lower than the buffer pump flow rate and so it plays no role in the overall flow rate of the CFFE. Both pumps have speed settings between 0.1 and 99.9 arbitrary units, but can be calibrated in terms of mL/min as described in the Instrument Calibrations and Maintenance section of this appendix. The pumps should be calibrated frequently, as over time the peristaltic tubing stretches and the flow rates change. One common problem with the buffer pump is maintaining similar flow rates for each line. All seven lines across the separation chamber should be flowing at approximately the same flow rate (within ~ 0.5 mL/min) for laminar flow to occur. If their flow rates vary too much, the buffer flow could become turbulent and not uniform. This typically results in samples deflecting or mixing and diffusing throughout the chamber, hindering separation. It is also recommended that all lines from the pump be primed with a disposable syringe in order to prevent air bubbles from blocking the flow solution in the lines.

A4.3 Power Supply

The power supply is responsible for generating the electric field used to separate samples across the chamber's width. The power supply is a Bertan 105-02R purchased from Spellman High Voltage with 2 kV and 1 Amp maximum settings. The power supply can be run with constant voltage or constant current while varying the other. Most experiments are run in constant voltage mode, since the current naturally changes as the buffer is depleted. It is important to note that the maximum voltages that can be used to separate analytes are greatly dependent on buffer composition. Low conductivity buffers, below 500 $\mu\text{S}/\text{cm}$, are best for use with the CFFE. This prevents electrolysis of the buffer which occurs when the current is too high. Only voltages that keep the current below 100-120 mA should be used to separate materials. If air bubbles begin to appear in the separation chamber or in either of the electrode chamber outlets, the current is probably too high for a uniform electric field to be generated.

A4.4 Fraction Collector

All solution inside the separation chamber will eventually end up in the fraction collector. The fraction collector is a series of 48 pieces of small tubing that is attached to the bottom of the separation chamber that leads to a large plastic array positioned on the right side of the separation chamber. Fitted styrofoam trays holding vials can be placed on an adjustable stage beneath the array for collection of sample. To keep sample volume low, it is recommended starting experiments with a large plastic bin under the fraction collector array. When the desired sample is nearing the bottom of the separation chamber, the plastic bin can be switched out for a tray of vials without having to halt the

separation. The inner diameter of the fraction collector tubing is small enough that even a little air bubble can block the flow of solution. Therefore it is recommended that prior to separation, the fraction collector tubing be primed using a blunt tipped HPLC injection needle and syringe to evacuate the air bubbles in each line. Air bubbles may still be present in the line even if solution is flowing.

A4.5 Cooling System

The cooling system consists of an array of capillary tubing strung vertically through out the separation chamber. Cold water from an ice bath is pumped up through the tubing, cooling the separation chamber down to 0°C. This is done to prevent joule heating which can cause disturbances or temperature gradients in the buffer flow, negatively affecting separation. Typical CFFE experiments last several hours, so multiple changes of ice is usually required to keep the chamber cooled.

A4.6 Outer Casing

The outer casing is designed as a safety precaution to prevent electrocution. This system is capable of lethal voltages and currents during electrophoretic separations. Caution is advised at any time the high voltage power supply is turned on. To prevent serious injury, a clear plastic shield has been designed to enclose the separation chamber when in use. A safety switch has been built into the casing to prevent the power supply from working without this shield in place, though it is still possible to access the separation chamber through a hole in the back of the casing. It is strongly suggested not to handle any part of the separation chamber while the high voltage is turned on.

A5 Instrumental Calibrations and Maintenance

In this section, we will cover important maintenance issues that can crop up during the use of the R&S CFFE instrument. As previously mentioned, there is no commercial access to replacement parts for this instrument and any such parts will need to be fabricated in the machine shop. Aside from the replacement of broken parts there are a number of disposable materials that will require replacement, as well as a few calibration experiments that will need to be performed from time to time.

A5.1 Pump Calibration

As mentioned previously, from time to time the buffer and sample pumps will require calibration to ensure that all lines flow at the same rate and to convert the pump settings into mL/min flow rates. It is recommended that the pumps be calibrated at least every time the peristaltic tubing is replaced if not more frequently. The first calibration to complete is to adjust the individual flow rates of all seven buffer lines on the buffer pump to the same flow rate. These flow rates should be as close as possible and certainly within ± 0.5 mL/min of each other. Use the follow procedure for individual line calibration:

- 1.) Collect effluent from a single line in a graduated cylinder for 2-5 minutes, recording time and volume to get flow rate in mL/min. Repeat for all seven separation chamber lines and all four electrode buffer lines.

- 2.) Adjust thumbscrew holding tubing in place to slow (tighten) or increase (loosen) the flow rate of each line and re measure the flow rate until all seven separation lines match and all four electrode lines match.

When the instrument is not in use, disconnect the tubing from the pump so that it is not stretched. This will make the tubing last longer and minimize the need to recalibrate.

To calibrate the flow rate of the overall CFFE system in terms of mL/min, the individual pump lines should have already been calibrated as described above. The pump needs to be hooked up to the CFFE like performing a separation experiment, but no high voltage is necessary. Like with the previous calibration, water will be collected from the fraction collector array in a plastic bin for a set time (5 minutes works well) and then measured with a large graduated cylinder. In this case a range of pump settings between 0.1 and 99.9 must be measured in order to construct a calibration curve similar to Figure A3. This curve can be used in later separation experiments to report flow rates in mL/min as opposed to the arbitrary units on the pump itself. The same procedure can be used to calibrate the sample pump as well.

Buffer Pump Calibration

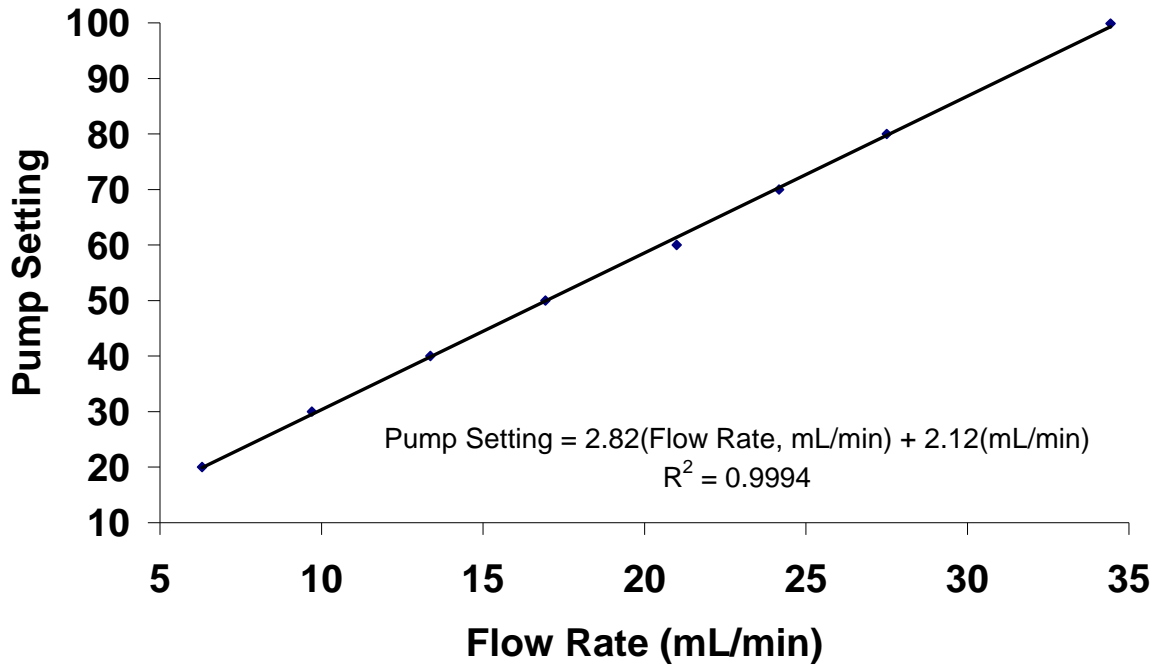


Figure A3. Example Buffer pump calibration curve plotting pump setting versus actual flow rates.

A5.2 Checking Flow Profile

Laminar flow is desired inside the separation chamber for CFFE experiments, though it is challenging to know if the flow is consistent across the chamber in a typical experiment. One way to check is to pump a different colored solution through each of the seven separation chamber inlet lines. This can be easily achieved, as each line can be placed in a different container of water that has been colored with food coloring. As the chamber fills with the colored water, the flow profile of each individual stream becomes apparent. If there is consistent flow across the chamber, straight bands of color should be readily visible running down the chamber. Any areas of turbulence, spreading, or thinning of the bands due to inconsistent flow rates will be visible. As seen in Figure A4, the colored streams arc to the right, leaving a clear area on the left side of the chamber. The flow profile can be corrected by re-adjusting the individual flow rates of the buffer pump lines to the same relative flow rates. As seen in Figure A5, once the flow rates are adjusted, the entire chamber is filled with colored solution that runs straight down the chamber with no arcing or deflecting. It is important to note two things about Figure A5, however. First, the bands of color seem to pinch in at the bottom of the chamber, and second new colors seem to be appearing in the lower corners of the chamber (green on the left, red on the right). Both of these phenomena are results of the physical characteristics of the bottom of the separation chamber which has only 48 small openings for the solution to fit through and so the solution backs up at the bottom. It is a good idea to check the flow profile occasionally to maintain optimal separation parameters.

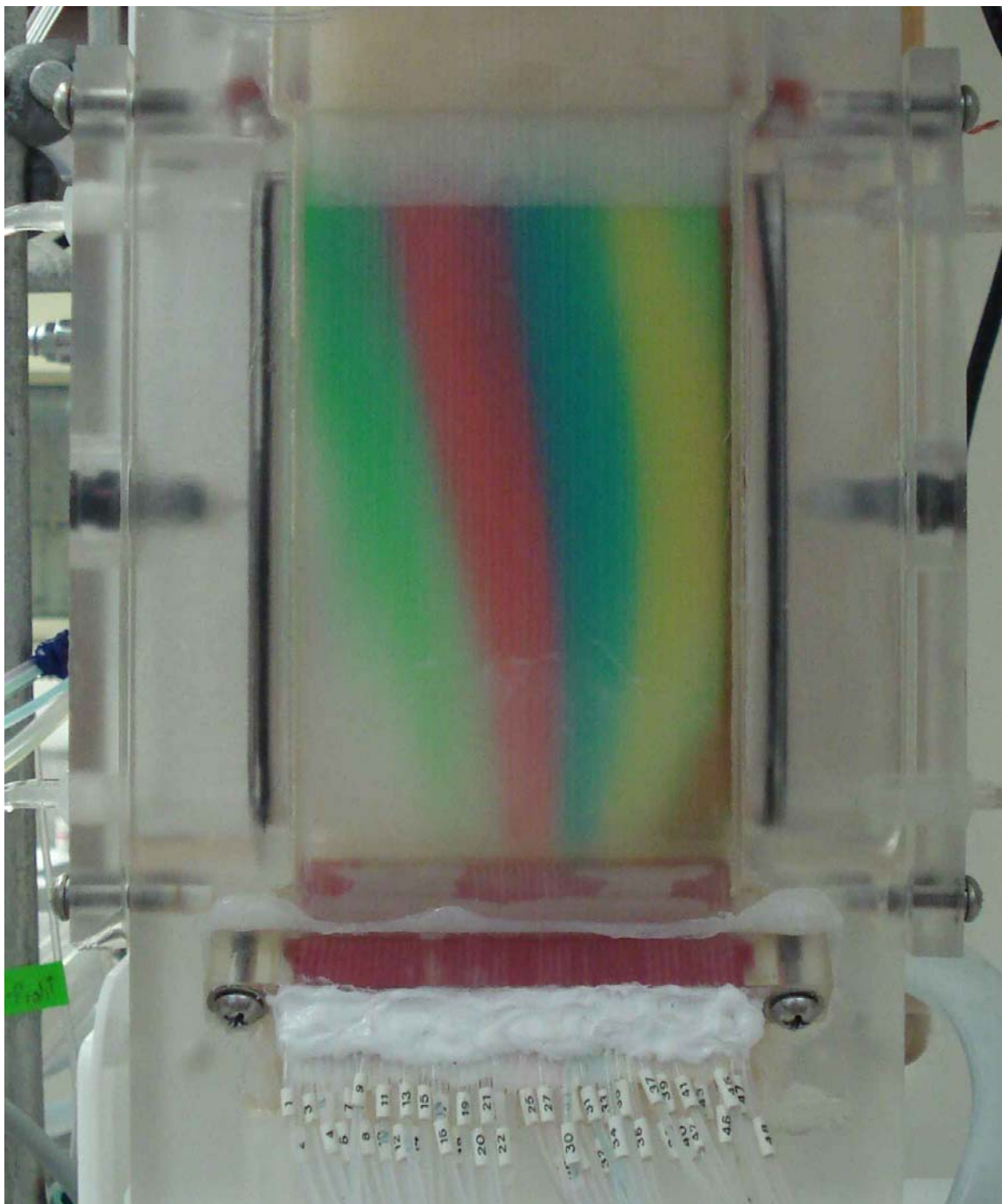


Figure A4. Picture of CFFE experiment checking the flow profile of solution inside the chamber. Here, flow of solution is non-uniform as evidenced by the clear area at the right of the chamber as well as the bending of the colored streams.



Figure A5. Picture of CFFE experiment checking the flow profile of solution inside the chamber. Here, flow of solution appears as uniform bands flowing straight down the chamber with no clear areas.

A5.3 Membrane Replacement

The nylon membrane that separates the electrode chamber from the main separation chamber should be replaced anytime any holes, rips, or discoloration are apparent. Plastic clips originally held the membrane taut against the lip of the electrode chamber. However, these clips were made of a brittle plastic, and broke very easily. Currently we use a combination of silicon sealant and rubber bands to attach the membrane to the electrode chamber. The membranes of both electrode chambers should be checked prior to every experiment.

To replace the electrode membrane:

- 1.) Remove rubber bands and o-rings from around the membrane lip.
- 2.) With a scalpel, carefully cut away the white sealant and membrane from a small area.
- 3.) Peel the membrane off the plastic lip and remove excess sealant by rubbing with a gloved hand. Make sure there is no excess sealant inside the plastic lip of the electrode chamber.
- 4.) Cut out a 4 x 15 cm rectangle of 0.45 μm nylon membrane.
- 5.) Apply a small amount of fresh sealant to the top of the plastic lip and gently place the new membrane on top, covering the entire opening.
- 6.) Cover the membrane with a small piece of paper and clamp it to a hard surface. Allow sealant to dry overnight.
- 7.) Unclamp the electrode chamber and carefully remove the paper. Carefully make small cuts in the excess membrane near the rounded ends of the chamber for better fitting.

- 8.) Apply a small bead of sealant along the side of the plastic lip all the way around.
- 9.) Carefully, starting at the long edges, fold the membrane down and stick it to the sealant, be extra careful around the rounded ends (You may have to make a few more cuts in the membrane for it to fit easily.).
- 10.) Secure the membrane with several rubber bands, making sure the membrane is moderately tight all the way around. Let dry overnight.
- 11.) Replace the o-rings and lightly grease the plastic sides of the electrode chamber with vacuum grease.
- 12.) Replace electrode chamber into CFFE and screw into place. Check for leaks the next time solution is pumped through the CFFE.

A6 Experimental Walkthrough

It is important to prepare everything needed for a separation experiment in advance. Once the separation experiment has begun, there is little time to devote to making more buffer, or setting up a tray of vials for fraction collection and the like. Take the time before the CFFE is started to get everything laid out and ready, even if this means preparing the day before a run. It is better to be over prepared than to have to stop an experiment in the middle due to poor planning. CFFE is a preparative scale separation technique and as such it takes a great amount of time to perform a single run. Plan to start a run as early in the day as possible, since once you have started, you cannot stop and come back to it later. This section will provide the reader with a detailed description of procedures used to operate the CFFE before, during, and after the separation experiment

A6.1 Buffer and Sample Preparation

First and foremost is the buffer and the sample to be separated. Make plenty of buffer. Buffer components are cheap, and it is better to have extra buffer left over than to run out in the middle of a separation. For most experiments, 10-20 liters of buffer should be sufficient. The composition of the buffer should be chosen depending on the sample to be separated, but generally needs to have a low conductivity (below 500 $\mu\text{S}/\text{cm}$). This is because high conductivities produce high electric currents which in turn can electrolyze the buffer and destabilize the separation. Due to the fact that neither component has counter ions, a common buffer system is tris (hydroxymethyl) aminomethane pH adjusted with boric acid.

When at all possible, it is best for the sample to be dissolved in the same buffer solution that will be used in the CFFE. Dissimilar solutions can inhibit initial separation of the sample until diluted in the separation buffer. For best results, sample concentrations should be as high as possible, since during the process of separation, the CFFE naturally dilutes samples $\sim 100\times$ their initial concentration. All samples should be filtered through a 0.45 μm syringe filter prior to injection.

A6.2 CFFE Setup

Once buffer and sample are prepared, the CFFE pumping system is ready to be setup. The buffer pump has a total of 9 lines that need to be primed prior to attaching them to the CFFE. Place the fritted ends of each line into the buffer reservoir and draw buffer through the peristaltic pump tubing with a disposable syringe until no air bubbles

remain. Then lock the peristaltic tubing in place on the pump. This removes air from the lines and assures that all lines will pump smoothly. The two electrode buffer lines that pump out of the separation chamber do not need to be primed. Instead, leave them unlocked on the pump until later. Next, attach the seven smaller separation chamber lines to the back of the separation chamber and attach the electrode buffer lines to each electrode chamber such that buffer is pumped in at the bottom and out at the top of each chamber. Once this is done, open the vent at the top back of the separation chamber and turn the buffer pump on at its highest setting. Allow the separation chamber to fill with buffer from the bottom up. Once buffer is freely flowing out of the two electrode buffer lines that were left open, lock down those lines and place them in a waste container for collection. When buffer is flowing out of the open vent, the separation chamber is filled and the vent can be plugged up. Once the vent is sealed again, buffer will begin to drip out of the fraction collector array on the left side of the instrument. Some lines might not be dripping. This is caused by air bubbles caught in the lines. Use a blunt tipped HPLC injection needle on a disposable syringe to apply a vacuum on each line to remove air bubbles. It is important to use the syringe on all 48 lines. Even if the line is dripping buffer, air bubbles may still be present and could cause blockages later. Once the buffer is freely flowing, reduce the buffer pump to the desired setting and let run for at least 30 minutes to 1 hour before separation. This time is to allow the flow profile of the system to stabilize and equilibrate.

Next, attach the sample pump to one of the three ports on the top of the separation chamber and seal the two unused ports. Place the end of the tubing in the sample and set

the flow rate of the sample pump to the desired flow rate. Leave the sample pump turned off.

While the pumping system is allowed to stabilize, fill the ice bath with water and ice and turn on the submersible pump. The ice bath keeps the temperature inside the separation chamber cool by pumping water through an array of capillary tubing that is strung vertically inside the separation chamber. This prevents joule heating which causes eddies and temperature gradients in the buffer at higher electric currents. Next, attach the electrodes to the electrode chambers and put the clear plastic shield in place over the separation chamber. Press the reset button on the front of the CFFE casing and turn on the power supply. Turn on the red high voltage switch and slowly increase the voltage to the desired setting. The system should be allowed to continue stabilizing as described above.

A6.3 Running the CFFE

After the CFFE has been allowed to equilibrate for about an hour, the sample pump can be started and the separation experiment begun. Once the sample has entered the chamber and separation has started, it must continue until finished. When the sample starts to reach the bottom of the chamber, place a tray with vials under the fraction collector array, making sure that the tubing is dripping into each vial. It is recommended to closely monitor the separation as it progresses. If the sample being separated is colored, taking pictures at various time points is an excellent way to document the separation. During the separation, be sure to top off the ice bath with fresh ice as needed.

A6.4 After CFFE Separation

Once the separation is complete, remove the fraction tray, turn off the power supply and detach the electrodes from the electrode chamber. Place the buffer pump on the highest setting and pump ~ 4 L of DI water through the system. This flushes out the buffer components to prevent it from crystallizing inside the CFFE. After the system has been flushed, detach the lines from the separation chamber and unlock the peristaltic tubing from the pump so it is not being stretched. Drain the separation chamber by removing one of the electrode chambers with a screw driver. The CFFE instrument should be stored in this state for prolonged periods of time.

REFERENCES

1. Templeton, A. C.; Chen, S. W.; Gross, S. M.; Murray, R. W., Water-soluble, isolable gold clusters protected by tiopronin and coenzyme A monolayers. *Langmuir* **1999**, *15* (1), 66-76.
2. Cliffel, D. E.; Zamborini, F. P.; Gross, S. M.; Murray, R. W., Mercaptoammonium-monolayer-protected, water-soluble gold, silver, and palladium clusters. *Langmuir* **2000**, *16* (25), 9699-9702.
3. Ackerson, C. J.; Jadzinsky, P. D.; Kornberg, R. D., Thiolate ligands for synthesis of water-soluble gold clusters. *J Am Chem Soc* **2005**, *127* (18), 6550-6551.
4. Brown, L. O.; Hutchison, J. E., Controlled growth of gold nanoparticles during ligand exchange. *J Am Chem Soc* **1999**, *121* (4), 882-883.
5. Porta, F.; Krpetic, Z.; Prati, L.; Gaiassi, A.; Scari, G., Gold-ligand interaction studies of water-soluble aminoalcohol capped gold nanoparticles by NMR. *Langmuir* **2008**, *24* (14), 7061-7064.
6. Stefanescu, D. M.; Glueck, D. S.; Siegel, R.; Wasylishen, R. E., Synthesis and characterization of phosphido-monolayer-protected gold nanoclusters. *Langmuir* **2004**, *20* (24), 10379-10381.
7. Balasubramanian, R.; Guo, R.; Mills, A. J.; Murray, R. W., Reaction of Au-55(PPh₃)(12)Cl-6 with thiols yields thiolate monolayer protected Au-75 clusters. *J Am Chem Soc* **2005**, *127* (22), 8126-8132.
8. Nuzzo, R. G.; Zegarski, B. R.; Dubois, L. H., Fundamental-Studies of the Chemisorption of Organosulfur Compounds on Au(111) - Implications for Molecular Self-Assembly on Gold Surfaces. *J Am Chem Soc* **1987**, *109* (3), 733-740.
9. Brust, M.; Walker, M.; Bethell, D.; Schiffrin, D. J.; Whyman, R., Synthesis of Thiol-Derivatized Gold Nanoparticles in a 2-Phase Liquid-Liquid System. *J Chem Soc Chem Comm* **1994**, (7), 801-802.
10. Hostetler, M. J.; Wingate, J. E.; Zhong, C. J.; Harris, J. E.; Vachet, R. W.; Clark, M. R.; Londono, J. D.; Green, S. J.; Stokes, J. J.; Wignall, G. D.; Glish, G. L.; Porter, M. D.; Evans, N. D.; Murray, R. W., Alkanethiolate gold cluster molecules with core diameters from 1.5 to 5.2 nm: Core and monolayer properties as a function of core size. *Langmuir* **1998**, *14* (1), 17-30.

11. Templeton, A. C.; Cliffel, D. E.; Murray, R. W., Redox and fluorophore functionalization of water-soluble, tiopronin-protected gold clusters. *J Am Chem Soc* **1999**, *121* (30), 7081-7089.
12. Alvarez, M. M.; Khoury, J. T.; Schaaff, T. G.; Shafiqullin, M. N.; Vezmar, I.; Whetten, R. L., Optical absorption spectra of nanocrystal gold molecules. *J Phys Chem B* **1997**, *101* (19), 3706-3712.
13. Brust, M.; Bethell, D.; Kiely, C. J.; Schiffrin, D. J., Self-assembled gold nanoparticle thin films with nonmetallic optical and electronic properties. *Langmuir* **1998**, *14* (19), 5425-5429.
14. Lee, D.; Donkers, R. L.; Wang, G. L.; Harper, A. S.; Murray, R. W., Electrochemistry and optical absorbance and luminescence of molecule-like Au-38 nanoparticles. *J Am Chem Soc* **2004**, *126* (19), 6193-6199.
15. Bigioni, T. P.; Whetten, R. L.; Dag, O., Near-infrared luminescence from small gold nanocrystals. *J Phys Chem B* **2000**, *104* (30), 6983-6986.
16. Huang, T.; Murray, R. W., Visible luminescence of water-soluble monolayer-protected gold clusters. *J Phys Chem B* **2001**, *105* (50), 12498-12502.
17. Wang, G. L.; Huang, T.; Murray, R. W.; Menard, L.; Nuzzo, R. G., Near-IR luminescence of monolayer-protected metal clusters. *J Am Chem Soc* **2005**, *127* (3), 812-813.
18. Wang, G. L.; Guo, R.; Kalyuzhny, G.; Choi, J. P.; Murray, R. W., NIR luminescence intensities increase linearly with proportion of polar thiolate ligands in protecting monolayers of Au-38 and Au-140 quantum dots. *J Phys Chem B* **2006**, *110* (41), 20282-20289.
19. Chen, S. W.; Murray, R. W.; Feldberg, S. W., Quantized capacitance charging of monolayer-protected Au clusters. *J Phys Chem B* **1998**, *102* (49), 9898-9907.
20. Hicks, J. F.; Templeton, A. C.; Chen, S. W.; Sheran, K. M.; Jasti, R.; Murray, R. W.; Debord, J.; Schaaf, T. G.; Whetten, R. L., The monolayer thickness dependence of quantized double-layer capacitances of monolayer-protected gold clusters. *Anal Chem* **1999**, *71* (17), 3703-3711.
21. Hicks, J. F.; Miles, D. T.; Murray, R. W., Quantized double-layer charging of highly monodisperse metal nanoparticles. *J Am Chem Soc* **2002**, *124* (44), 13322-13328.
22. Wuelfing, W. P.; Green, S. J.; Pietron, J. J.; Cliffel, D. E.; Murray, R. W., Electronic conductivity of solid-state, mixed-valent, monolayer-protected Au clusters. *J Am Chem Soc* **2000**, *122* (46), 11465-11472.

23. Eklund, S. E.; Cliffel, D. E., Synthesis and catalytic properties of soluble platinum nanoparticles protected by a thiol monolayer. *Langmuir* **2004**, *20* (14), 6012-6018.
24. Templeton, A. C.; Wuelfing, M. P.; Murray, R. W., Monolayer protected cluster molecules. *Accounts Chem Res* **2000**, *33* (1), 27-36.
25. Mooradia, A., Photoluminescence of Metals. *Phys Rev Lett* **1969**, *22* (5), 185-&.
26. Zheng, J.; Zhang, C. W.; Dickson, R. M., Highly fluorescent, water-soluble, size-tunable gold quantum dots. *Phys Rev Lett* **2004**, *93* (7), -.
27. Huang, T.; Murray, R. W., Quenching of [Ru(bpy)₃]²⁺ fluorescence by binding to Au nanoparticles. *Langmuir* **2002**, *18* (18), 7077-7081.
28. Gerdon, A. E.; Wright, D. W.; Cliffel, D. E., Epitope mapping of the protective antigen of B-anthraxis by using nanoclusters presenting conformational peptide epitopes. *Angew Chem Int Edit* **2006**, *45* (4), 594-598.
29. Gerdon, A. E.; Wright, D. W.; Cliffel, D. E., Quartz crystal microbalance detection of glutathione-protected nanoclusters using antibody recognition. *Anal Chem* **2005**, *77* (1), 304-310.
30. Neiman, B.; Grushka, E.; Lev, O., Use of gold nanoparticles to enhance capillary electrophoresis. *Anal Chem* **2001**, *73* (21), 5220-5227.
31. Bucking, W.; Nann, T., Electrophoretic analysis of gold nanoparticles: size-dependent electrophoretic mobility of nanoparticles. *Iee Proc-Nanobiotech* **2006**, *153* (3), 47-53.
32. Ivanov, M. R.; Bednar, H. R.; Haes, A. J., Investigations of the mechanism of gold nanoparticle stability and surface functionalization in capillary electrophoresis. *ACS Nano* **2009**, *3* (2), 386-94.
33. Templeton, A. C.; Hostetler, M. J.; Kraft, C. T.; Murray, R. W., Reactivity of monolayer-protected gold cluster molecules: Steric effects. *J Am Chem Soc* **1998**, *120* (8), 1906-1911.
34. Brust, M.; Fink, J.; Bethell, D.; Schiffrin, D. J.; Kiely, C., Synthesis and Reactions of Functionalized Gold Nanoparticles. *J Chem Soc Chem Comm* **1995**, (16), 1655-1656.
35. Templeton, A. C.; Hostetler, M. J.; Warmoth, E. K.; Chen, S. W.; Hartshorn, C. M.; Krishnamurthy, V. M.; Forbes, M. D. E.; Murray, R. W., Gateway reactions to diverse, polyfunctional monolayer-protected gold clusters. *J Am Chem Soc* **1998**, *120* (19), 4845-4849.

36. Watson, K. J.; Zhu, J.; Nguyen, S. T.; Mirkin, C. A., Hybrid nanoparticles with block copolymer shell structures. *J Am Chem Soc* **1999**, *121* (2), 462-463.
37. Hostetler, M. J.; Templeton, A. C.; Murray, R. W., Dynamics of place-exchange reactions on monolayer-protected gold cluster molecules. *Langmuir* **1999**, *15* (11), 3782-3789.
38. Donkers, R. L.; Song, Y.; Murray, R. W., Substituent effects on the exchange dynamics of ligands on 1.6 nm diameter gold nanoparticles. *Langmuir* **2004**, *20* (11), 4703-4707.
39. Hostetler, M. J.; Green, S. J.; Stokes, J. J.; Murray, R. W., Monolayers in three dimensions: Synthesis and electrochemistry of omega-functionalized alkanethiolate-stabilized gold cluster compounds. *J Am Chem Soc* **1996**, *118* (17), 4212-4213.
40. Holm, A. H.; Ceccato, M.; Donkers, R. L.; Fabris, L.; Pace, G.; Maran, F., Effect of peptide ligand dipole moments on the redox potentials of Au-38 and Au-140 nanoparticles. *Langmuir* **2006**, *22* (25), 10584-10589.
41. Song, Y.; Jimenez, V.; McKinney, C.; Donkers, R.; Murray, R. W., Estimation of size for 1-2 nm nanoparticles using an HPLC electrochemical detector of double layer charging. *Anal Chem* **2003**, *75* (19), 5088-5096.
42. Jimenez, V. L.; Leopold, M. C.; Mazzitelli, C.; Jorgenson, J. W.; Murray, R. W., HPLC of monolayer-protected gold nanoclusters. *Anal Chem* **2003**, *75* (2), 199-206.
43. Wei, G. T.; Liu, F. K.; Wang, C. R. C., Shape separation of nanometer gold particles by size-exclusion chromatography. *Anal Chem* **1999**, *71* (11), 2085-2091.
44. Wei, G. T.; Liu, F. K., Separation of nanometer gold particles by size exclusion chromatography. *J Chromatogr A* **1999**, *836* (2), 253-260.
45. Wilcoxon, J. P.; Martin, J. E.; Provencio, P., Size distributions of gold nanoclusters studied by liquid chromatography. *Langmuir* **2000**, *16* (25), 9912-9920.
46. Wilcoxon, J. P.; Martin, J. E.; Provencio, P., Optical properties of gold and silver nanoclusters investigated by liquid chromatography. *Journal of Chemical Physics* **2001**, *115* (2), 998-1008.
47. Schaaff, T. G.; Knight, G.; Shafiqullin, M. N.; Borkman, R. F.; Whetten, R. L., Isolation and Selected Properties of a 10.4 kDa Gold:Glutathione Cluster Compound. *J Phys Chem B* **1998**, *102* (52), 10643-10646.

48. Schaaff, T. G.; Whetten, R. L., Giant gold-glutathione cluster compounds: Intense optical activity in metal-based transitions. *J Phys Chem B* **2000**, *104* (12), 2630-2641.
49. Hanauer, M.; Pierrat, S.; Zins, I.; Lotz, A.; Sonnichsen, C., Separation of nanoparticles by gel electrophoresis according to size-and shape. *Nano Lett* **2007**, *7* (9), 2881-2885.
50. Schnabel, U.; Fischer, C. H.; Kenndler, E., Characterization of colloidal gold nanoparticles according to size by capillary zone electrophoresis. *Journal of Microcolumn Separations* **1997**, *9* (7), 529-534.
51. Liu, F. K.; Lin, Y. Y.; Wu, C. H., Highly efficient approach for characterizing nanometer-sized gold particles by capillary electrophoresis. *Anal Chim Acta* **2005**, *528* (2), 249-254.
52. Liu, F. K.; Wei, G. T., Adding sodium dodecylsulfate to the running electrolyte enhances the separation of gold nanoparticles by capillary electrophoresis. *Anal Chim Acta* **2004**, *510* (1), 77-83.
53. Liu, F. K.; Tsai, M. H.; Hsu, Y. C.; Chu, T. C., Analytical separation of Au/Ag core/shell nanoparticles by capillary electrophoresis. *J Chromatogr A* **2006**, *1133* (1-2), 340-346.
54. Liu, F. K., A high-efficiency capillary electrophoresis-based method for characterizing the sizes of Au nanoparticles. *J Chromatogr A* **2007**, *1167* (2), 231-235.
55. Lo, C. K.; Paau, M. C.; Xiao, D.; Choi, M. M. F., Capillary electrophoresis, mass spectrometry, and UV-visible absorption studies on electrolyte-induced fractionation of gold nanoclusters. *Anal Chem* **2008**, *80* (7), 2439-2446.
56. Lo, C. K.; Paau, M. C.; Xiao, D.; Choi, M. M. F., Application of capillary zone electrophoresis for separation of water-soluble gold monolayer-protected clusters. *Electrophoresis* **2008**, *29* (11), 2330-2339.
57. Peterson, R. R.; Cliffel, D. E., Continuous free-flow electrophoresis of water-soluble monolayer-protected clusters. *Anal Chem* **2005**, *77* (14), 4348-4353.
58. Canut, H.; Bauer, J.; Weber, G., Separation of plant membranes by electromigration techniques. *J Chromatogr B* **1999**, *722* (1-2), 121-139.
59. Hoffmann, P.; Wagner, H.; Weber, G.; Lanz, M.; Caslavská, J.; Thormann, W., Separation and purification of methadone enantiomers by continuous- and interval-flow electrophoresis. *Anal Chem* **1999**, *71* (9), 1840-1850.

60. Hoffstetterkuhn, S.; Kuhn, R.; Wagner, H., Free-Flow Electrophoresis for the Purification of Proteins .1. Zone Electrophoresis and Isotachopheresis. *Electrophoresis* **1990**, *11* (4), 304-309.
61. Clifton, M. J.; Jouve, N.; Debalman, H.; Sanchez, V., Conditions for Purification of Proteins by Free-Flow Zone Electrophoresis. *Electrophoresis* **1990**, *11* (11), 913-919.
62. Weber, G.; Bocek, P., Optimized continuous flow electrophoresis. *Electrophoresis* **1996**, *17* (12), 1906-1910.
63. Stalcup, A. M.; Sutton, R. M. C.; Painuly, P.; Rodrigo, J. V.; Gratz, S. R.; Yanes, E. G., Continuous free flow electrophoresis for preparative chiral separations of piperoxan using sulfated beta-cyclodextrin. *Analyst* **2000**, *125* (10), 1719-1724.
64. Schneiderman, E.; Gratz, S. R.; Stalcup, A. M., Optimization of preparative electrophoretic chiral separation of ritalin enantiomers. *J Pharmaceut Biomed* **2002**, *27* (3-4), 639-650.
65. Gratz, S. R.; Schneiderman, E.; Mertens, T. R.; Stalcup, A. M., Use of dyes to investigate migration of the chiral selector in CFFE and the impact on the chiral separations. *Anal Chem* **2001**, *73* (16), 3999-4005.
66. Sanganza, W. K. M.; Ridgway, T. H.; Stalcup, A. M.; Seliskar, C. J., An online fiber-optic UV-visible detector for continuous free-flow electrophoresis. *Electrophoresis* **2005**, *26* (22), 4270-4276.
67. Brauer, G., *Handbook of Preparative Inorganic Chemistry*. New York, 1965; p p 1054.
68. Ingram, R. S.; Hostetler, M. J.; Murray, R. W., Poly-hetero-omega-functionalized alkanethiolate-stabilized gold cluster compounds. *J Am Chem Soc* **1997**, *119* (39), 9175-9178.
69. Landers, J. P., *Handbook of capillary electrophoresis*. 2nd ed.; CRC Press: Boca Raton, 1997; p 894 p.
70. Guo, R.; Song, Y.; Wang, G. L.; Murray, R. W., Does core size matter in the kinetics of ligand exchanges of monolayer-protected Au clusters? *J Am Chem Soc* **2005**, *127* (8), 2752-2757.
71. Arnaud, I.; Abid, J. P.; Roussel, C. R.; Girault, H. H., Size-selective separation of gold nanoparticles using isoelectric focusing electrophoresis (IEF). *The Royal Society of Chemistry 2005 Communication* **2005**, 787-788.

72. Kohlmann, O.; Steinmetz, W. E.; Mao, X. A.; Wuelfing, W. P.; Templeton, A. C.; Murray, R. W.; Johnson, C. S., NMR diffusion, relaxation, and spectroscopic studies of water soluble, monolayer-protected gold nanoclusters. *J Phys Chem B* **2001**, *105* (37), 8801-8809.